Geomorphology 280 (2017) 89–107

Contents lists available at ScienceDirect

Geomorphology

journal homepage: www.elsevier.com/locate/geomorph

Glacial geomorphology of the northwestern Weddell Sea, eastern Antarctic Peninsula continental shelf: Shifting ice flow patterns during deglaciation

Jennifer M. Campo [a,*], Julia S. Wellner [a], Eugene Domack [b], Caroline Lavoie [c], Kyu-Cheul Yoo [d]

[a] Department of Earth and Atmospheric Sciences, University of Houston, Houston, TX 77204, USA
[b] College of Marine Science, University of South Florida, St. Petersburg, FL 33701, USA
[c] CESAM/Department of Geosciences, University of Aveiro, Aveiro 3810-193, Portugal
[d] Korea Polar Research Institute, Incheon 406-840, South Korea

ARTICLE INFO

Article history:
Received 17 June 2016
Received in revised form 30 November 2016
Accepted 30 November 2016
Available online 3 December 2016

Keywords:
Submarine glacial geomorphology
Ice flow patterns
Multibeam data
Antarctica Peninsula
Weddell Sea

ABSTRACT

During the Last Glacial Maximum, grounded ice from the expanded Antarctic Peninsula Ice Sheet extended across the continental shelf. Grounded and flowing ice created a distinctive array of glacial geomorphic features on the sea floor, which were then exposed as the ice sheet retreated. The recent disintegration of the northern parts of the Larsen Ice Shelf (Larsen A and B) have permitted acquisition of marine geophysical data in previously inaccessible and unmapped areas. We present a reconstruction of the evolving ice-flow path and ice sheet geometry of the eastern Antarctic Peninsula, with particular focus paid to newly surveyed areas that shed light on the dynamics of a marine-terminating glacial geomorphic environment, where ice shelves play a major role in grounding line stability. Shifting flow directions were mapped in several areas, including across the Seal Nunataks, which divide Larsen A and B, and offshore of Larsen C, indicating flow reorientation that reflects the changing ice sheet geometry as retreat neared the modern coastline. The measured flow indicators in this area reveal comparatively high elongation ratios (>20), indicating rapid ice flow. Evidence of possible previous ice-shelf collapses are noted near the shelf break, further illustrating the critical, protective effect that ice shelves impart to marine-terminating glacial environments. Modern ice retreat is governed in part by reorganization of flow patterns accompanying grounding line movement; such reorganizations happened in the past and can aid understanding of modern processes.

1. Introduction

The Antarctic Peninsula (AP; study area shown in Fig. 1) is composed of a thin, elongate backbone (>250 km wide, 1250 km long) of rugged mountains capped by an estimated thickness range of 400 to 800 m of ice (Zagorodnov et al., 2012; Fretwell et al., 2013). The mountains form an orographic barrier to the westerly winds, resulting in a polar-maritime climate in the western AP and in a polar-continental climate with westerly downslope föhn winds (Grosvenor et al., 2014) over the eastern AP. The study area presented extends from 63.5° to 66.5° South latitude.

The AP is a rapidly warming region, with an increase of 3.7 ± 0.7 °C over the last 60 years (Vaughan et al., 2003) and is sensitive to climate fluctuations, owing in part to its northern position and to the relatively small size of its glaciers compared to the West and East Antarctic Ice Sheets. The vulnerability of the AP to external environmental conditions produces observable responses to climatic changes on the decade to century time scale (Bentley, 1999; Evans et al., 2005). During the Last Glacial Maximum (LGM), when ice was last expanded to its maximum position around the globe, the Antarctic Peninsula Ice Sheet (APIS) extended to the outer shelf, with some areas reaching the continental shelf break (Anderson et al., 2002; Heroy and Anderson, 2005, 2007). During the subsequent deglaciation, the grounded ice of the APIS began to retreat to its current interglacial position. This retreat contributed an estimated 1.7 m to global sea-level rise (Bentley, 1999), while simultaneously shedding sediment onto the outer shelf, forming distinct geomorphic and sediment assemblages that record the rate and style of ice movement (Pudsey, 2000; Wellner et al., 2001; Ó Cofaigh et al., 2002; Evans et al., 2005; Heroy and Anderson, 2005). Flowing grounded ice carved a distinctive array of geomorphic features into the sea floor. The grounded ice eventually decoupled from the sea floor and transitioned into the fringing ice shelves on the eastern side of the AP and small glaciers terminating below sea level on the western

* Corresponding author.
E-mail address: jmcampo@mac.com (J.M. Campo).

http://dx.doi.org/10.1016/j.geomorph.2016.11.022
0169-555X/

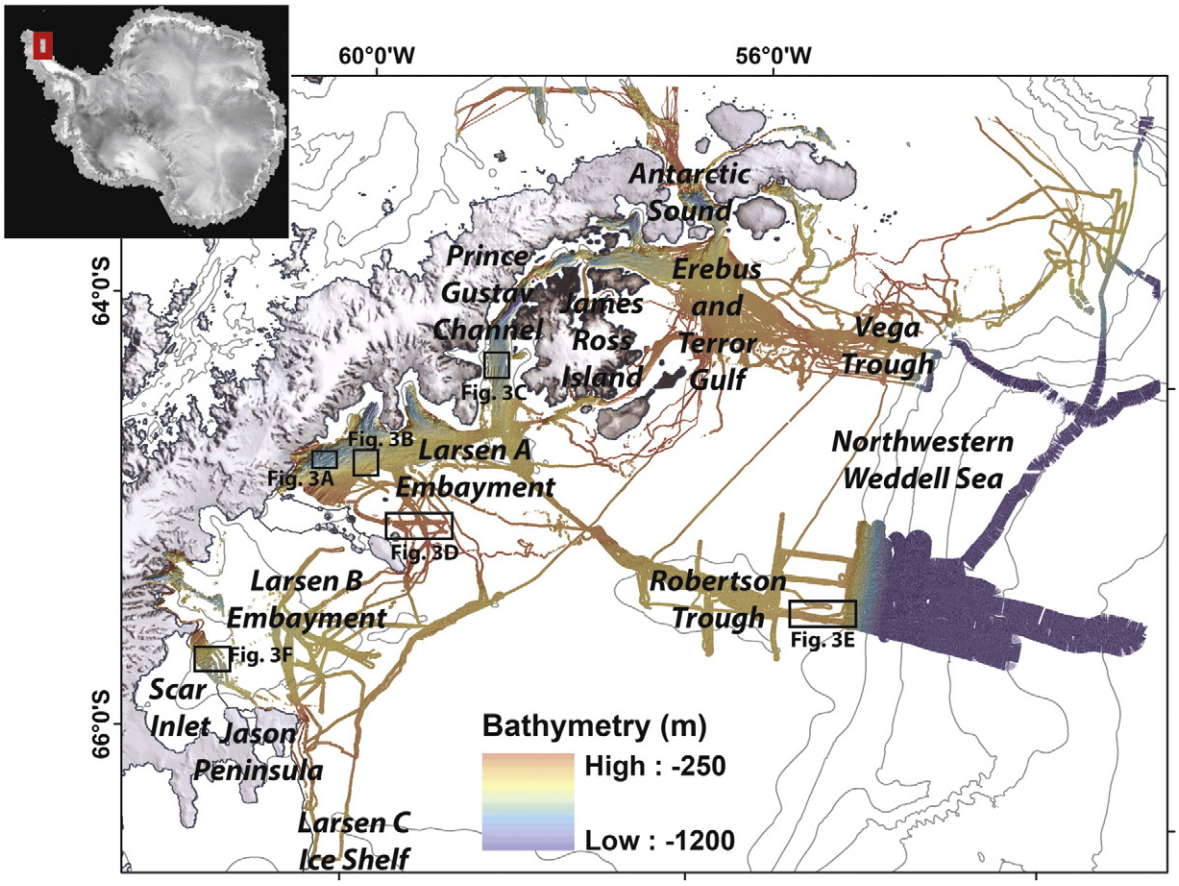

Fig. 1. Location map of the eastern AP and multibeam swath bathymetry data set (gridded at 25 m) from USAP, British Antarctic Survey, and Korea Polar Research Institute surveys; background land image, 30-m spatial resolution, from Landsat Image Mosaic of Antarctica (LIMA); dark gray line shows coastline and ice shelf extent, from British Antarctic Survey (BAS); light gray lines show bathymetric contour interval of 500 m from IBSCO (Arndt et al., 2013). Black boxes show location of geomorphic feature examples shown in Fig. 3.

side of the Peninsula (Brachfeld et al., 2003; Domack et al., 2005). The subglacial geomorphic features described in the following sections likely began to develop prior to the LGM, and development continued throughout the time that ice was grounded at any given location. Features formed by erosion of bedrock likely represent several glacial-interglacial cycles. On the other hand, each readvance of the ice will obliterate sedimentary features in relatively short time. Thus, the sedimentary structures observed on the shelf represent a snapshot of subglacial conditions just prior to ice retreat from any location (e.g., Anderson et al., 2001; Wellner et al., 2006).

Relict subglacial geomorphology is a powerful tool for interpreting past glacial flow patterns (e.g., Clark, 1993; Canals et al., 2000; Wellner et al., 2001; Spagnolo et al., 2016). Geomorphic mapping from multibeam swath bathymetry data from across the Antarctic continental shelf has allowed reconstruction of the past extent of the Antarctic Ice Sheet across many portions of the continental shelf and demonstrated a common set of geomorphic features that are used to interpret ice-flow patterns (Canals et al., 2000; Wellner et al., 2001, Wellner et al., 2006; Dowdeswell et al., 2004; Domack et al., 2006, Klages et al., 2015; Lavoie et al., 2015; Livingstone et al., 2016). The Robertson paleo-Ice Stream has been studied previously by many authors (e.g., Domack et al., 2001; Pudsey, 2000; Camerlenghi et al., 2001; Gilbert et al., 2003; Evans et al., 2005; Johnson et al., 2011; Davies et al., 2012a,b; Ó Cofaigh et al., 2014; Lavoie et al., 2015) and was thought to have been primarily active through the Larsen A embayment (see Fig. 1 for location), which is a focal point in this study (Domack et al., 2001), while also acting as catchment to ice lost southward through the Prince Gustav Channel (Camerlenghi et al., 2001). Here, we show a detailed reconstruction of the broader region made possible by the combined data sets, highlighting the role of bathymetric controls on retreat patterns. A focus was placed on mapping and measuring all geomorphic features within the data set. Previous studies

Table 1
Acoustic facies identified in CHIRP data.

Assignment	Description	Designation
Seismic facies 1	Bright seabed reflector with underlying parallel reflector, indicating relatively thin (1–10 m) sediment drape over acoustically chaotic unit	Minimal sediment accumulation over hard bottom
Seismic facies 2	Single hard reflector over acoustically chaotic unit with strong bowtie or hummocky reflections, generally proximal to coastline	Crystalline basement
Seismic facies 3	Acoustically chaotic unit with strong surface reflections and no internal reflections, smooth topography, generally located in mid-shelf environments	Subglacial till
Seismic facies 4	Multiple continuous and parallel reflections	Sediment deposition, basin fill, or drift deposit
Seismic facies 5	Asymmetric wedge with internal reflections	Drumlins composed of sediment overlying subglacial till
Seismic facies 6	Asymmetric wedge with no internal reflections	Grounding zone features, bedrock and till drumlins, crag-and-tails

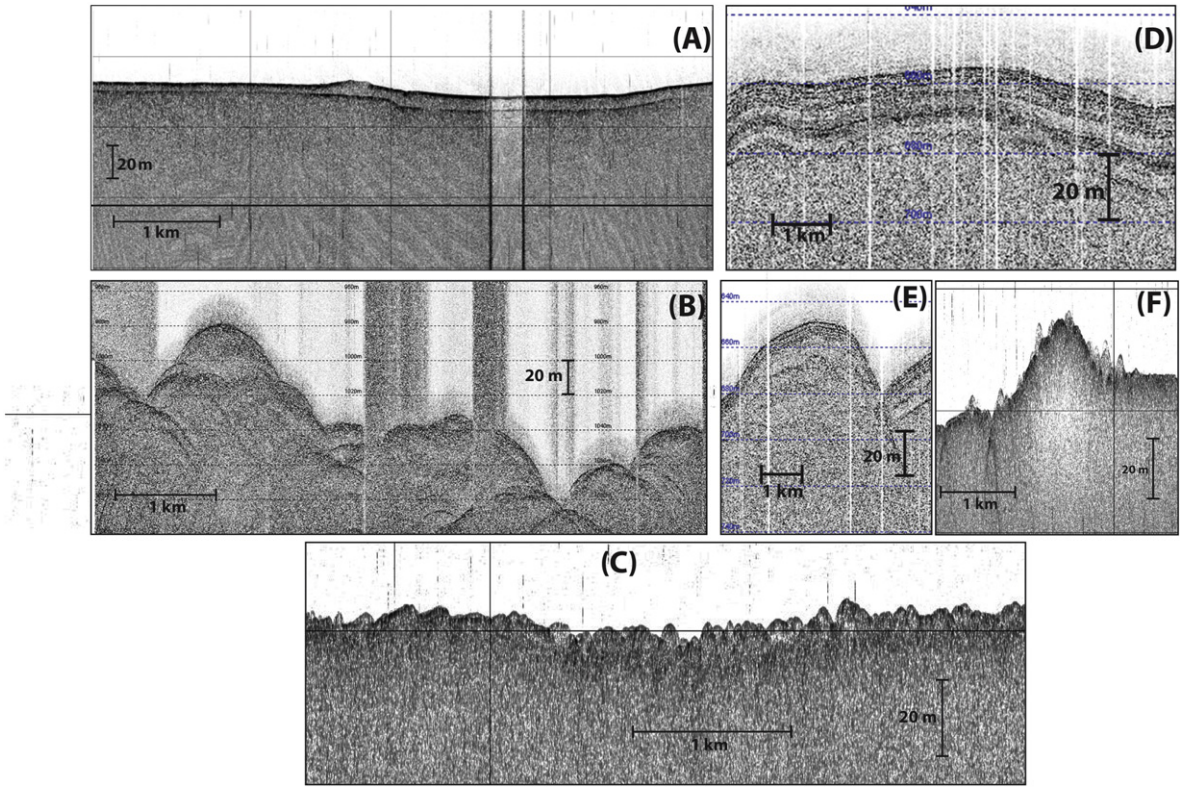

Fig. 2. CHIRP seismic facies classification: (A) seismic facies 1; (B) seismic facies 2; (C) seismic facies 3; (D) seismic facies 4; (E) seismic facies 5; (F) seismic facies 6.

have been localized in singular areas (e.g., Gilbert et al., 2003; Rebesco et al., 2014) or mapped generally to contribute to a regional context (e.g., Lavoie et al., 2015). In this study, each feature in the compiled data set was mapped and measured in order to capture the glacial retreat history of the northeastern AP in detail.

The bed under the current Antarctic Ice Sheet is difficult to access or image, and thus details of the geological controls on flow are hard to determine. However, the seafloor where ice has been grounded during the last glacial-interglacial cycle records past flow conditions in the geomorphology (e.g., Canals et al., 2000; Stokes and Clark, 2002; Domack et al., 2006; Wellner et al., 2006) and in the distribution of sedimentary facies (e.g., Wellner et al., 2001; Shipp et al., 2002; Ó Cofaigh et al., 2005; Livingstone et al., 2016). Models combining the two suggest mechanisms for sediment transport and geomorphic feature development tied to ice dynamics (e.g., Clark et al., 2003). Detailed reconstructions of past flow patterns, like the one offered here, can better constrain

Table 2
Geomorphic mapping classes and criteria for identification.

GIS mapping class	Mapped landform	Defining characteristics	Study example	Count
Roches moutonées		Asymmetric bedrock hills, abraded stoss (up-ice) faces, quarried lee faces	Exasperation inlet	69
Glacial lineations	MSGLs	≥1 km long, width 200–1300 m, $\varepsilon > 10$, parallel sets of ridges and grooves in deformable substrate (till) with amplitudes between 1 and 9 m	Larsen A and B embayment, Fig. 3B, C, F	1642
	Flutings	≥100 m long, width 50–1000 m, $\varepsilon < 10$, parallel sets of ridges and grooves in deformable substrate (till), sometimes with curved paths	Larsen A embayment, Fig. 3D	222
Drumlinoid features	Drumlins	Streamlined landforms, tear-drop or ovoid shaped. Stoss end is up-ice indicator. Depositional and erosional formation, tend to form in swarms	Greenpeace Trough	999
Erosional marks	Iceberg furrows	Curvilinear furrows and grooves (≤100 m width) formed in sediment and deformable substrate at varying depths. No discernible pattern of geometry or orientation	Seal Nunataks, Fig. 3E	3126
	Striations	Erosional features incised into bedrock by direct glacial action	Drygalski Trough	302
	Grooves	Occur in bedrock by direct subglacial abrasion or in deformable substrate either by iceberg keel ploughing or by glacial action. Often ≥10 km long, ≥100 m wide	Larsen C system	277
Grounding zone features		Wedge-shaped sediment package, indicating still-stand or period of stasis in glacial activity, up to tens of m high	Larsen A embayment, Fig. 3B	476
Meltwater channels		Linear to sinuous channels primarily cut into bedrock but are sometimes observed forming around stoss heads of drumlins in sediment. May form anastomosing networks that span several km	Larsen A embayment	476
Unidentified erosional features		Repeating chain of ridges and grooves, set in curvilinear pattern, perpendicular to ice flow	Scar inlet	90

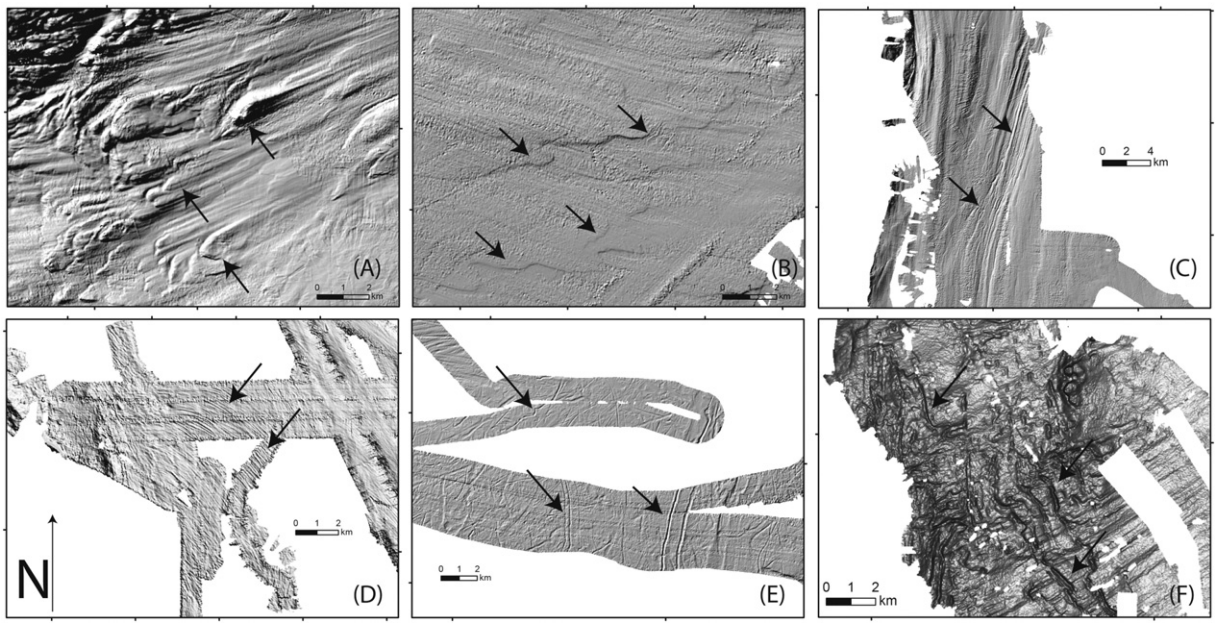

Fig. 3. Geomorphic features on relief-shaded, bathymetric maps. Locations of the features are shown in Fig. 1. Black arrows indicate the glacial features. For classification criteria, please refer to Table 2. North is to the top of the page, as indicated in (D). (A) Drumlin swarm (previously mapped by Gilbert et al., 2003), highly attenuated with some superposition, trend to the northwest, in Greenpeace Trough, Larsen A embayment (no exaggeration, shaded from the northwest); (B) grounding zone lobes and MSGLs, trend to the southeast, in the Larsen A embayment (no exaggeration, shaded from the northwest); (C) MSGLs in the Prince Gustav Channel, trend to the south (no exaggeration, shaded from the northwest); (D) flutings showing a curving pattern to the southeast, north of Robertson Island in the Larsen A embayment (exaggeration of 25, shaded from the northeast); (E) iceberg furrows, scours, and grooves, east of the Larsen B embayment (no exaggeration, shaded from the northwest); (F) unidentified erosional features and MSGLs in Scar Inlet (exaggeration of 45, shaded from above).

models of flow conditions during past glacial expansions and are thus a critical piece of the story of glacial history of a region (cf., Golledge et al., 2013).

2. Methods

Geophysical data has been compiled from several U.S. Antarctic Program research cruises (NBP0003, NBP0107, NBP0201, NBP0502, NBP0602A, NBP0603, NBP0703, NBP1001, NBP1203), a British Antarctic Survey cruise (JR071), and the most recent data from a Korea Polar Research Institute (KOPRI) cruise (AR1304). Multibeam swath bathymetry data from this compilation was used to generate an extensive bathymetric map of the northeastern region of the AP continental shelf. The CHIRP subbottom profiles were taken to estimate rock and sediment types of the geomorphic assemblages and general shelf composition. Multibeam data surveys from the Alfred Wegener Institute within the Larsen B Ice Shelf area and adjacent to the current Larsen C Ice Shelf system, as previously seen in the reconstruction presented by Lavoie et al. (2015), are not included in the maps presented here. That data has been presented in the past, but with limited digital availability and was not available for use in this study. The most recent data sets from AR1304 and NBP1203 are presented here — the multibeam collected during these cruises have previously been shown by Lavoie et al. (2015); however, the finely mapped detail, as well as the matching CHIRP profiles, are shown here for the first time.

2.1. Multibeam swath bathymetry data

The more recent multibeam data collected aboard the research vessel/ice breaker (RV/IB) *Araon* was acquired using a hull-mounted Kongsberg-Simrad EM-122 multibeam echosounder, with a swath of 432 beams and an operating frequency of 12 kHz. Data acquired aboard the RV/IB Araon was manually edited to remove errant data with the multibeam editing software CARIS HIPS&SIPS 8.0, and gridded to 25 × 25 m. The resulting grids were then imported into ArcMAP 10.1 and merged with preexisting maps to a shared grid size of 25 × 25 m. Previously collected multibeam surveys aboard the RV/IB *Nathaniel B.*

Table 3
Measurements of geomorphic flow indicators on the eastern AP.

Location	Measured landform	Length (m) min, mean, max	Width (m) min, mean, max	Spacing (m) min, mean, max	ε mean, max	*n*
Larsen A	Drumlins	298, 171, 821	62, 210, 475	n/a	4.6, 9.9	548
	Flutings	333, 1739, 7474	18, 82, 147	54, 96, 140	31, 94	222
	MSGLs	801, 4218, 15,302	144, 240, 510	n/a	18, 73	404
Larsen B	Drumlins	241, 949, 3079	68, 261, 776	n/a	4.1, 15	98
	MSGLs	364, 2896, 19,231	119, 242, 60	49, 91, 163	12, 101	592
Larsen C	Drumlins	289, 821, 1712	62, 210, 475	n/a	4.6, 9.9	23
	MSGLs	561, 1596, 2273	180, 294, 501	85, 138, 225	6, 11	22

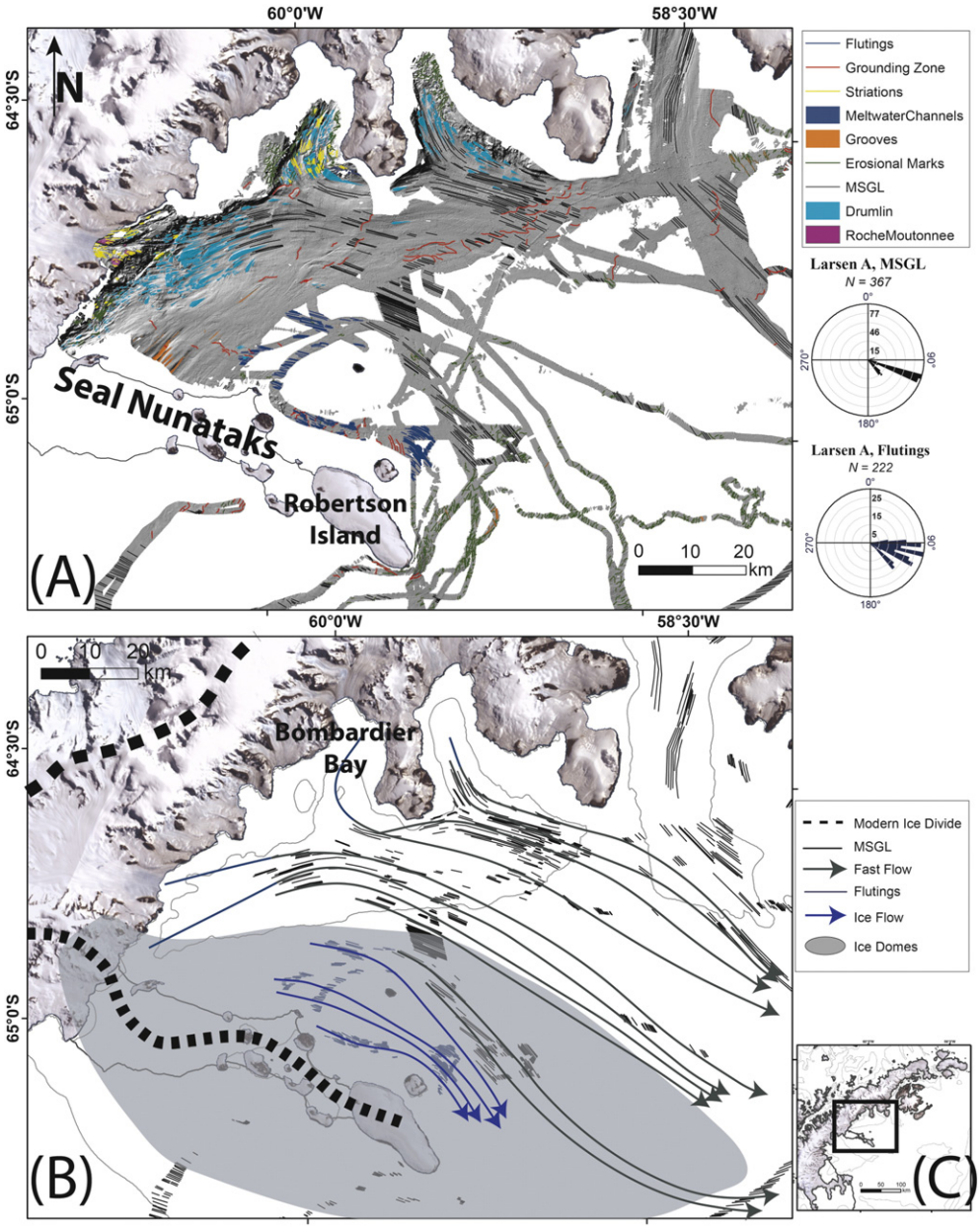

Fig. 4. Larsen A embayment: (A) Relief-shaded bathymetric map with no exaggeration, shaded from the northwest. Inner labels of the rose diagram correspond to the bin value of all azimuthal data at each reference circle level. (B) Ice streaming and flow map for the Larsen A embayment. Gray arrows indicate fast, or streaming, ice flow. Blue arrows indicate general ice flow direction. Gray polygons indicate ice domes, after Lavoie et al. (2015). Black dashed lines indicate the modern ice divide. (C) Location of Larsen A embayment on the AP. Background images by LIMA, bathymetric contour interval of 500 m from IBSCO (Arndt et al., 2013).

Palmer and the RRS *James Clark Ross* were collected with a hull-mounted Kongsberg-Simrad EM-120. This process generated high-resolution images of the submarine geomorphic features mapped in this study. Edge effect and multibeam artifact was noted within the compiled maps, and great care was taken to distinguish it from any geomorphic features. The artifact is very distinctive and characteristic and at no point did it appear parallel to any linear features or otherwise interfere with the mapping process.

2.2. CHIRP subbottom profiler

Along with the multibeam data, CHIRP data was collected during the entirety of the AR1304 cruise in 2013, to allow subbottom interpretation of features. High-resolution seismic surveys were conducted with swept frequencies centered at 3.5 kHz. The subbottom profiles were used to identify and characterize the sediment packages and bedrock beneath the sea floor. Sedimentary units as thin as 80 cm can be imaged, up to a maximum depth of approximately 100 m (Anderson et al., 2001). The CHIRP profiles were collected aboard the RV/IB Araon using a hull-mounted Kongsberg Maritime SBP120. Profiles were analyzed using the TOPAS viewer software from Kongsberg-Maritime SBP1.4.8. Additional CHRIP data was used from cruise NBP1203, collected about the RV/IB Palmer using a Knudsen 320B/R. Other legacy 3.5 kHz data from previous cruises has not been incorporated in this study owing to limited data access and file incompatibility.

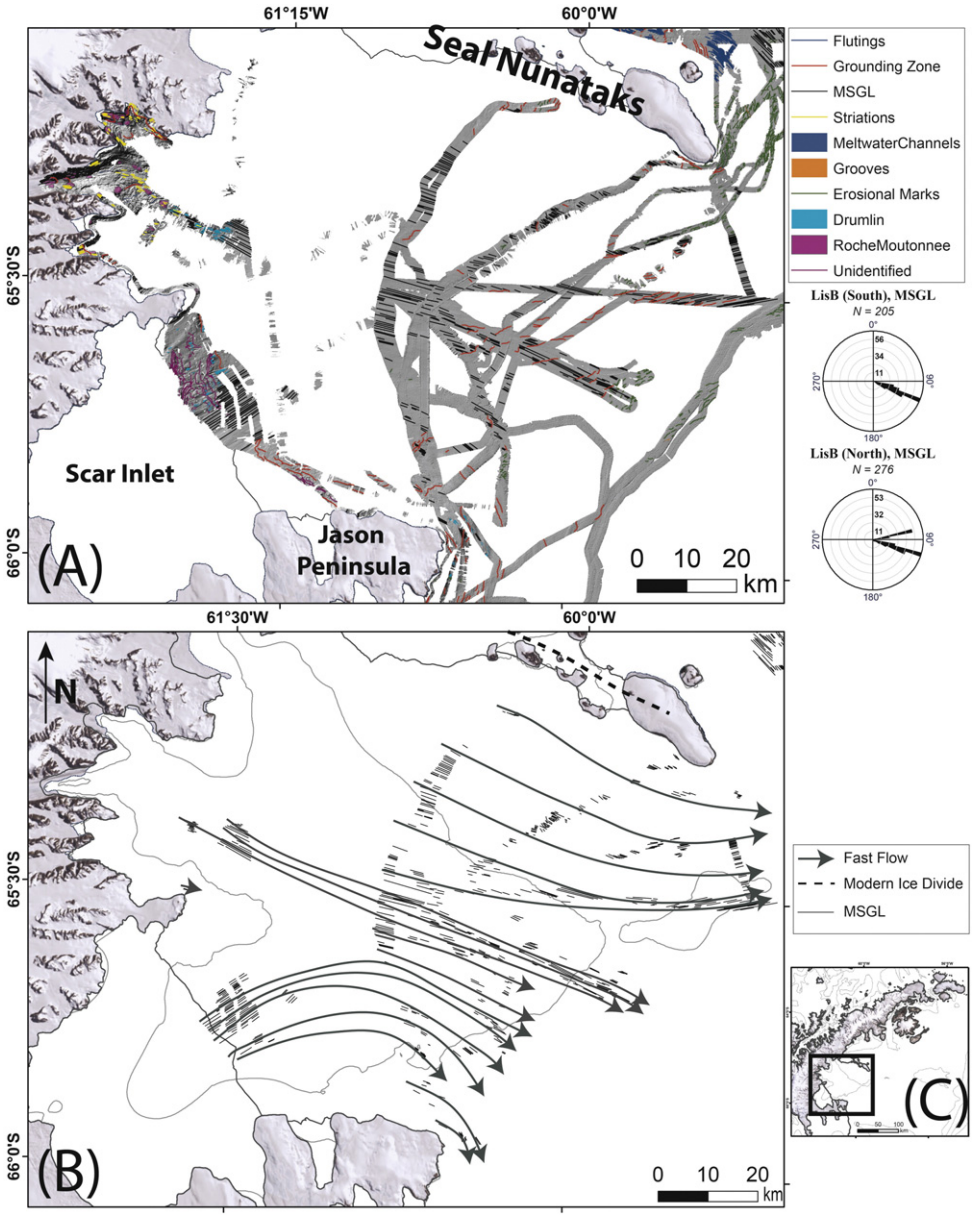

Fig. 5. Larsen B embayment: (A) Relief-shaded bathymetric map with no exaggeration, shaded from the northwest; inner labels of the rose diagram correspond to the bin value of all azimuthal data at each reference circle level. (B) Ice streaming and flow map for the Larsen B embayment. Gray arrows indicate fast, or streaming, ice flow. Black dashed lines indicate the modern ice divide. (C) Location of Larsen B embayment on the AP. Background images by LIMA, bathymetric contour interval of 500 m from IBSCO (Arndt et al., 2013).

3. Feature mapping and interpretation

The CHIRP profiles were analyzed for reflection types and divided into six facies based on their acoustic character, as described in Table 1 and shown in Fig. 2. Bathymetric data was used to observe the seafloor geometries and compare to glacial geomorphology described in other marine locations as well as on land. Seven major glacial landform types were identified based on observed geometries and then further subdivided: roches moutonnées, megascale glacial lineations (MSGLs), drumlinoid features (drumlins, crag-and-tails), erosional marks (iceberg scours and furrows, striations, grooves), grounding zones (wedges, lobes), meltwater channels, and unidentified erosional features. Geomorphic assemblages were mapped and classified according to the criteria presented in Table 2; examples are shown in Fig. 3. Features were mapped in ArcMap 10.1, using line and polygon feature classes to record lengths and, where appropriate, widths and perimeters. Elongation ratios of glacial features were calculated using the equation $\varepsilon =$ length/width. Tabular results for measured MSGL and drumlin features of each major area are shown in Table 3.

3.1. Geomorphic assemblages in the Larsen A embayment

The glacial troughs near the coastline of the Larsen A embayment (Fig. 1; cf., Lavoie et al., 2015) are characterized by hummocky and irregular surfaces, while the mid-to outer shelf environment is fluted and generally smooth. Iceberg furrows become predominant features off the coast of Robertson Island and remain significant parts of the landscape out to the shelf break, indicative of the open marine conditions following deglaciation (Heroy and Anderson, 2005). The CHIRP profiles taken in newly surveyed coastal bays and troughs primarily

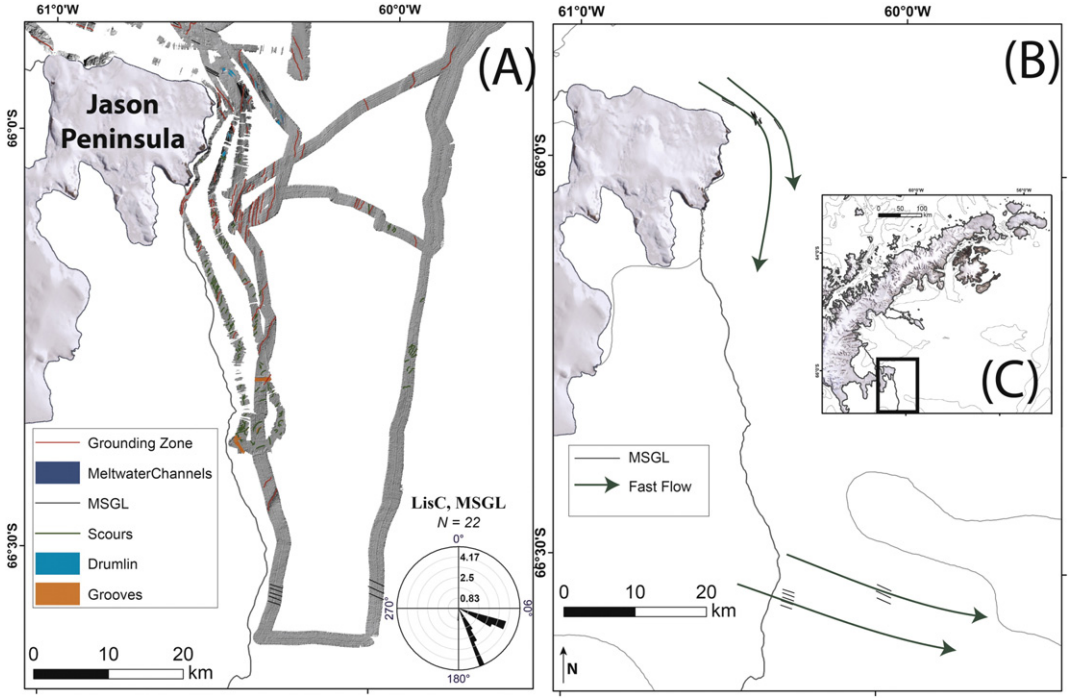

Fig. 6. Larsen C Ice Shelf system: (A) Relief-shaded bathymetric map with no exaggeration, shaded from the northwest; inner labels of the rose diagram correspond to the bin value of all azimuthal data at each reference circle level. (B) Ice streaming and flow map for the Larsen C Ice Shelf system. Gray arrows indicate fast, or streaming, ice flow where they overlie MSGLs. (C) Location of Larsen C Ice Shelf system on the AP. Background images by LIMA, bathymetric contour interval of 500 m from IBSCO (Arndt et al., 2013).

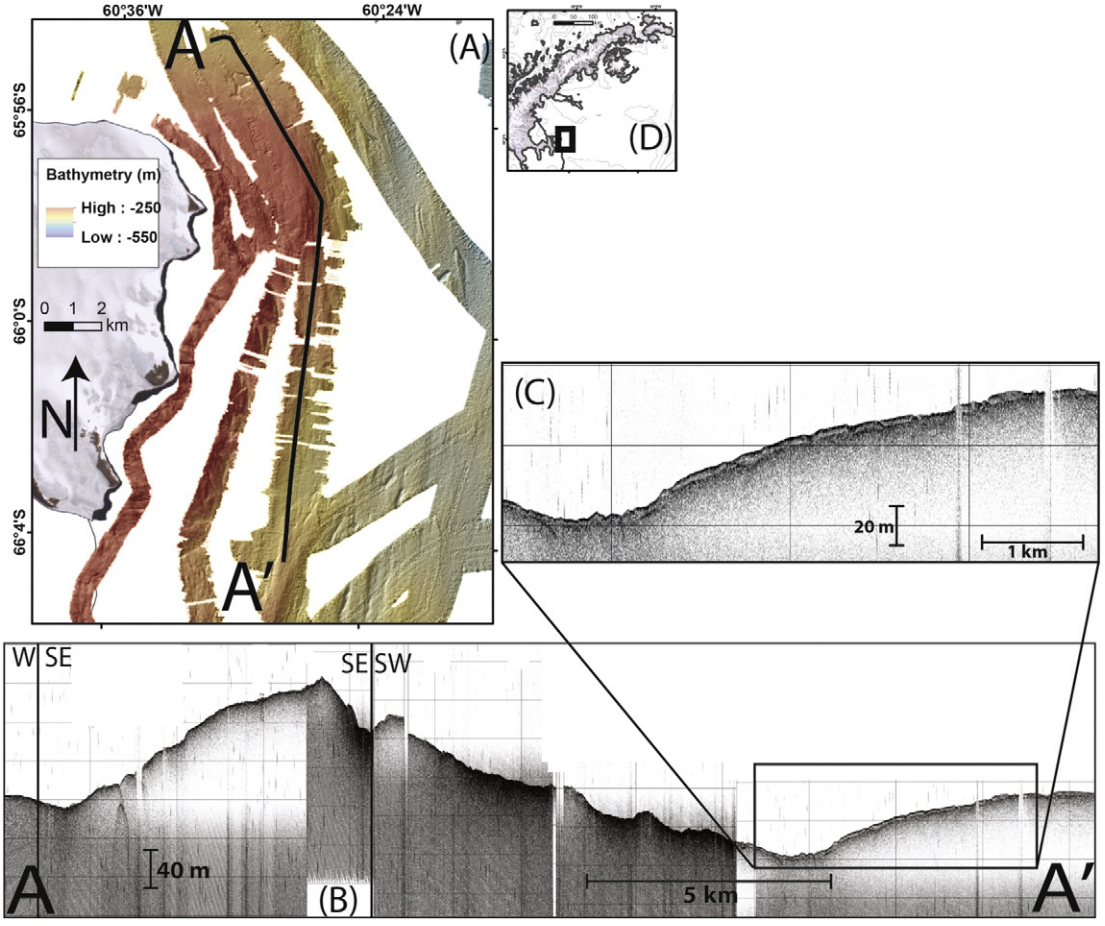

Fig. 7. Northern Larsen C Ice Shelf system: (A) Shaded relief map, showing subbottom profiles line A–A′. (B) Uninterpreted subbottom profile A–A′, vertical exaggeration is 55:1. (C) Close-up inset of sediment package from A–A′. (D) Location of CHIRP line on the AP.

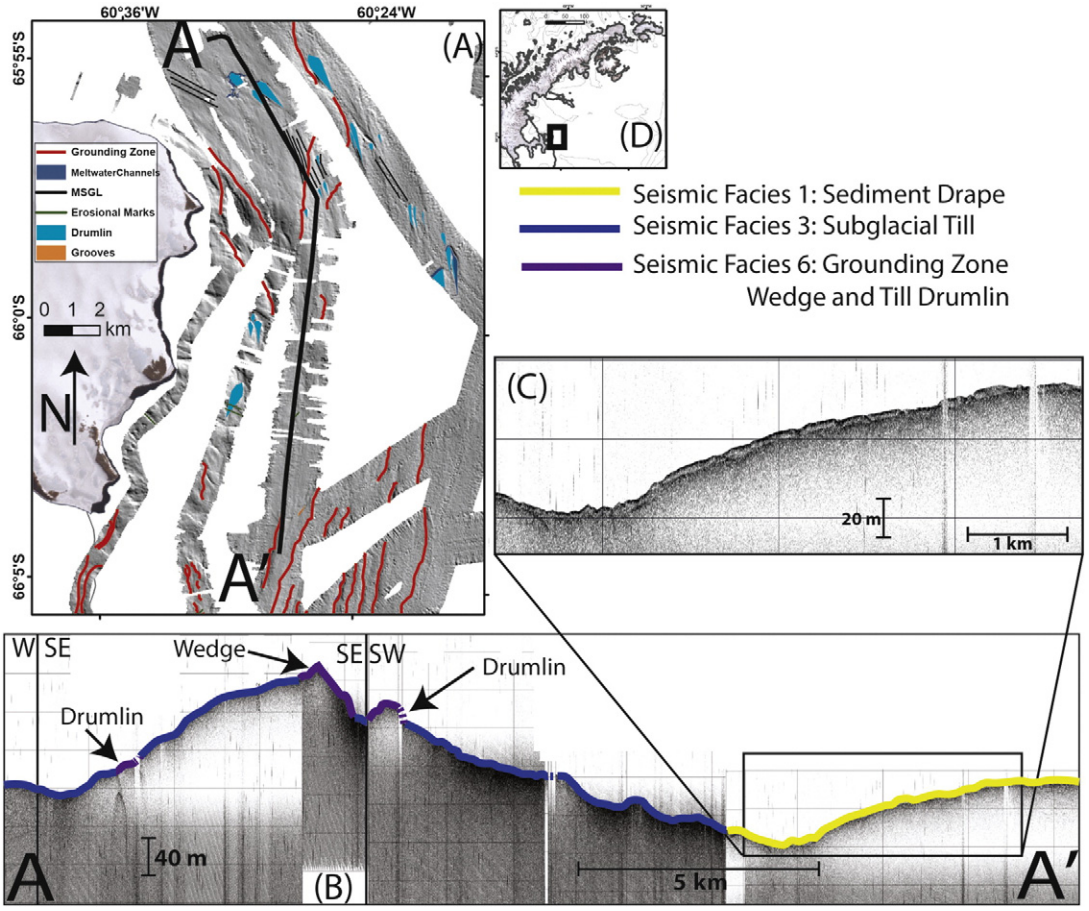

Fig. 8. (A) Interpretation of the shaded relief map, showing subbottom profile location for line A–A′. (B) Interpreted subbottom profile A–A′, mapped as seismic facies 1 (yellow), 3 (blue), and 6 (purple); vertical exaggeration is 55:1. (C) Close-up inset of sediment package from A–A′. (D) Location of CHIRP line on the AP.

show acoustically chaotic units, indicating a crystalline basement substrate in the inner fjords and coastlines. The CHIRP lines taken across the mid-shelf and outer shelf areas show subglacial till deposits. The submarine glacial geomorphic features of the Larsen A embayment were mapped and interpreted to show ice flow direction with an estimation of general velocity (Fig. 4). The MSGLs indicate fast ice flow, while drumlins are interpreted to indicate the onset of ice flow acceleration (Wellner et al., 2001; King et al., 2007). Directional data is presented using rose diagrams (Fig. 4).

Fast ice flow in the Larsen A embayment is clearly indicated by the presence of MSGLs and is largely shown to drain outward from the embayment to the southeast (arrows in Fig. 4). Sluggish ice flow was indicated by lack of elongated geomorphic features northeast of the Seal Nunataks, indicating ice flow beneath an ice mass but not within an active ice stream. This classification was made on the basis of the presence of deglacial lineations that fall well short of the expected geometric range for MSGLs (>1 km; Clark, 1993). Ice flows outward from Nordenskjold Coast and is topographically controlled in the outlet glacial trough of the Larsen A embayment (Fig. 4).

Inner shelf drumlinoid bedforms are strongly topographically controlled and reflective of changes in overlying glacial stresses, strength of the bed material (Rose and Letzer, 1977), and directional influence from changing and competing flow geometries over time. Within the confined fjord system, each outlet glacier can essentially act as a separate ice stream, exerting control from directly at the ice-bed interface within the glacial trough. If more than one outlet stream is draining an ice mass into a bay, the competing flow geometries may influence the shape of the subglacial bedforms over time or enhance the likelihood of superimposing bedforms on top of bedforms (Clark, 1993). We have mapped a cluster of at least six irregularly shaped, superimposed drumlins, which decrease in size toward the interior, within BDE Trough (located in Bombardier Bay (Fig. 4), which empties to the south into the Larsen A embayment).

3.2. Geomorphic assemblages in the Larsen B embayment

Ice flow in the Larsen B embayment (Fig. 5) shows two distinct flow assemblages, one in the northern area of the embayment and the other in the south.

The northern flow set emanates from the coastline in a southeasterly direction and turns briefly northeast (Fig. 5), before converging eastward with flow from the Larsen A embayment and Prince Gustav Channel, which had flow to the south in LGM time (e.g., Glasser et al., 2014; Nývlt et al., 2014). This particular set is most likely related to the Hektoria, Green, and Evans outlet glacial system and was obstructed by the Robertson Dome situated over the Seal Nunataks (Lavoie et al., 2015). The southern MSGL flow sets are oriented to the southeast (Fig. 5). A transect from north to south of the Larsen B embayment shows that the southeastern flow orientation becomes increasingly strong. Flow sets emanating northeast from Scar Inlet turn sharply southward near the tip of the Jason Peninsula. Fast flow is indicated throughout the Larsen B embayment, beginning at the transition from inner to

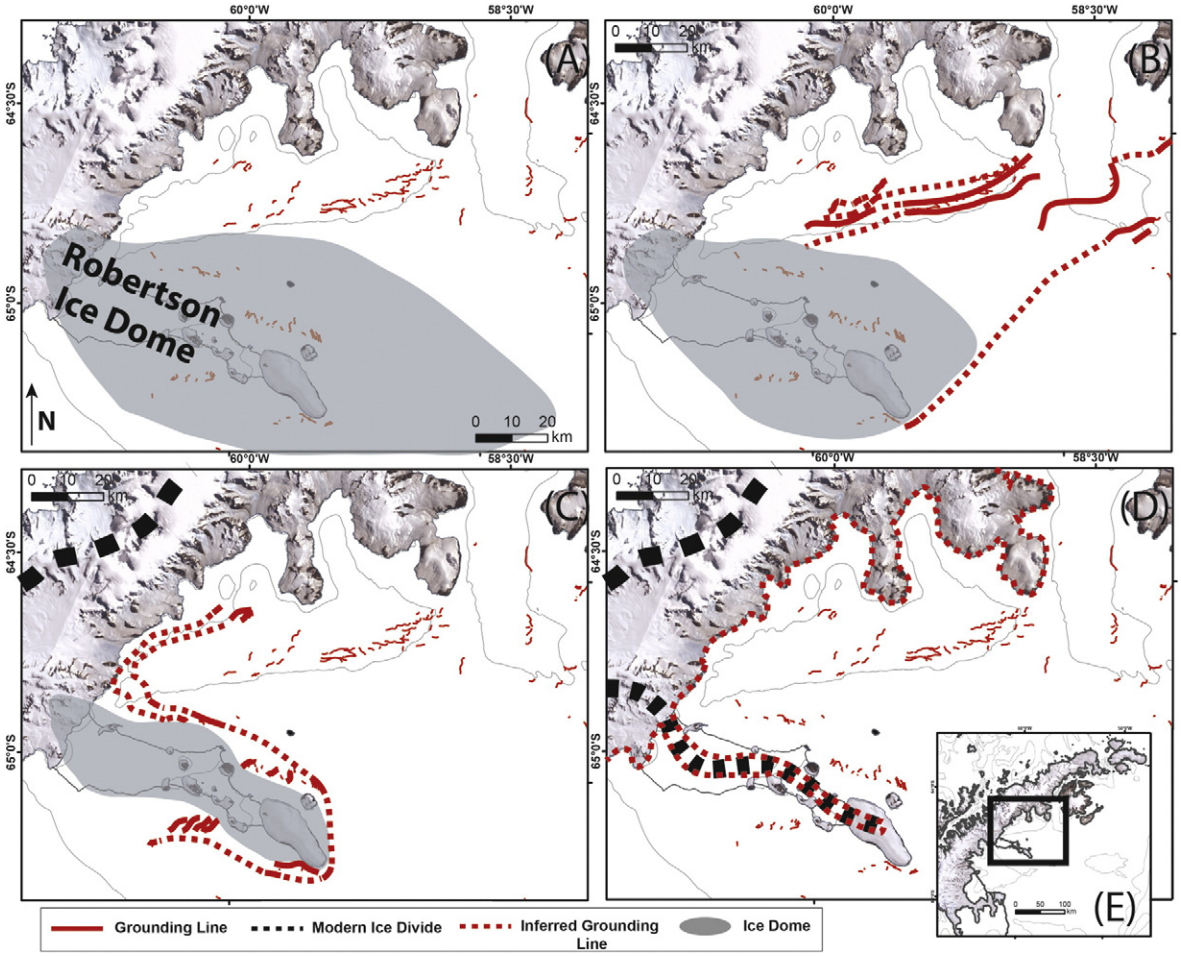

Fig. 9. Grounding line reconstruction for the Larsen A embayment. Solid red thin and thick lines indicate mapped grounding zone features; dashed red line indicates inferred grounding zone features. Black dashed lines indicate the modern ice divide; gray areas show locations of proposed ice domes (after Lavoie et al., 2015). (A) At the LGM, the entire region was covered by grounded ice; (B) early retreat grounding line geometry; (C) later retreat grounding line geometry; (D) estimated modern day grounding line; (E) location of Larsen A embayment on the AP. Background images by LIMA; bathymetric contour interval of 500 m from IBSCO (Arndt et al., 2013).

mid-shelf environment where more elongate landforms (drumlins, MSGLs) become the primary features. While the multibeam coverage in the Larsen B embayment is sparse, wherever coverage is present in the mid- to outer shelf environment, we have noted that MSGLs and grounding zones are the predominant features.

3.3. Geomorphic assemblages in the Larsen C Ice Shelf system

Ice flow in the Larsen C Ice Shelf system is largely constrained to the south and southeast (Fig. 6). The data collected in this region over the years is very sparse because of extensive sea ice and general inaccessibility — new findings are reported here for the first time.

Absence of MSGLs is notable in this area; in the northern portion of the survey area, only a few southeast-trending MSGLs were mapped, occasionally punctuated by grounding zone features. A CHIRP profile (Figs. 7 and 8) collected in the northern portion of the Larsen C system revealed a primarily mid-shelf environment composed of subglacial till (seismic facies 3 in Fig. 2; Fig. 8). A thick sediment drape (identified as such by its single reflection) ~4.5 m thick is noted on the right side of the profile (seismic facies 1 in Fig. 2; Fig. 8).

Beyond the tip of the Jason Peninsula, the coastline of this area is not strongly topographically controlled. In the southern portion, several MSGLs were mapped extending southeast from the Larsen C Ice Shelf (Fig. 6). Steep changes in slope are interpreted as grounding zone features with a primary northeastern orientation. This flow set is the only indication of fast flow south of the Jason Peninsula. All other mapped features suggest sluggish ice flow.

4. Discussion

4.1. Grounding line dynamics

4.1.1. Larsen A embayment

All outlet glacial flows of the Larsen A embayment eventually converge to the southeast in the mid-to outer shelf. Mapped grounding zones (Fig. 9) indicate a gradual deglacial history of the ice sheet, with several kilometers separating each grounding zone wedge.

The reorganization of grounding zone features from a northeastern (older configuration) to a northwestern (younger) orientation reflects the changing ice mass geometry as the centralized Robertson ice dome located over the Seal Nunataks continued to drain and shrink contemporaneously with the AP Ice Sheet and eventually with the modern, smaller AP Ice Cap.

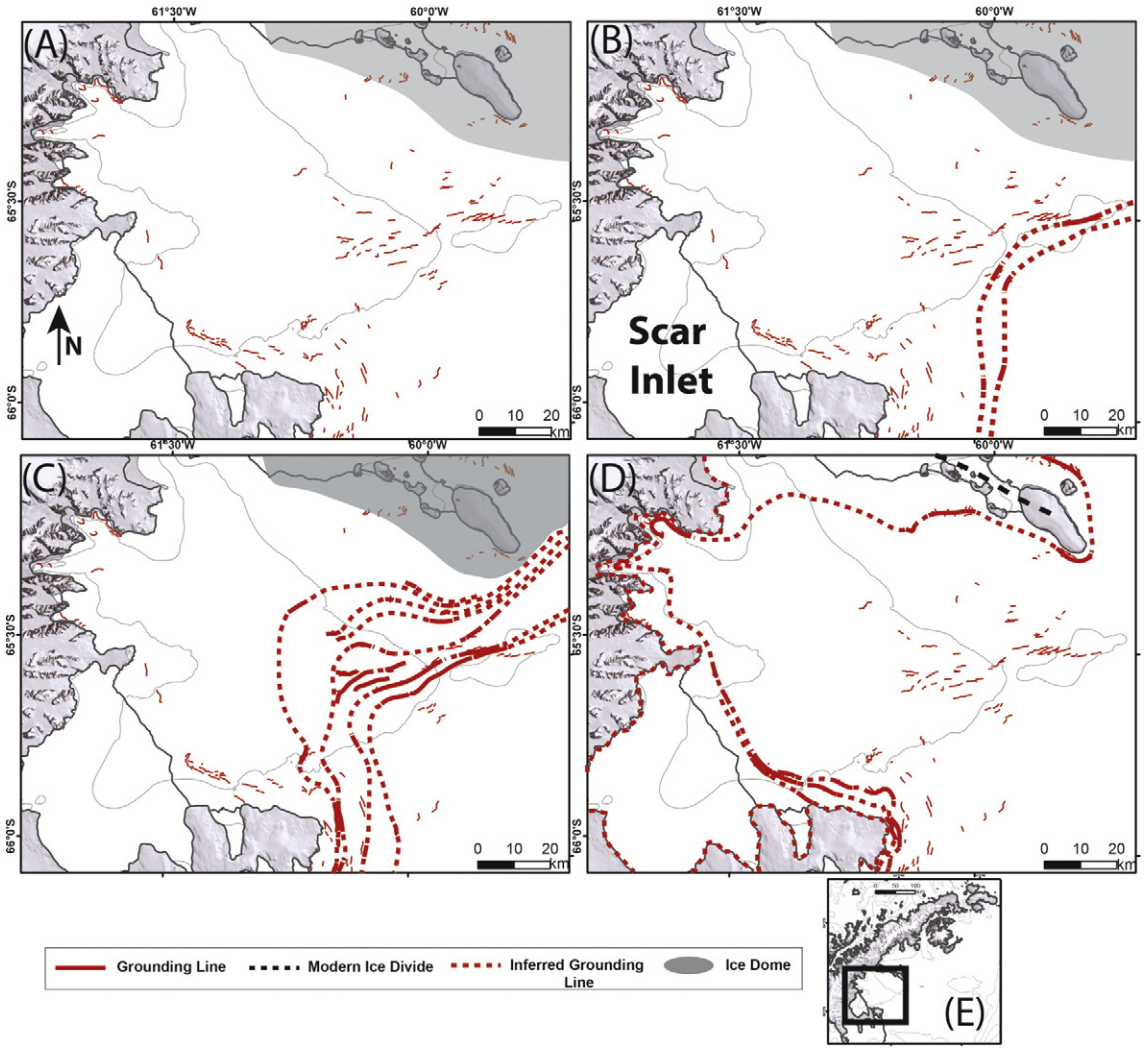

Fig. 10. Grounding line reconstruction for the Larsen B embayment. Solid thin and thick red lines indicate mapped grounding zone features; dashed red line indicates inferred grounding zone features. Black dashed lines indicate the modern ice divide; gray areas show locations of proposed ice domes (after Lavoie et al., 2015). (A) At the LGM, the entire region was covered by ice. (B) early stages of deglacial geometry; (C) later stages of deglacial geometry; (D) latest deglacial grounding lines and estimated modern day grounding line; (E) location of Larsen B embayment on the AP. Background images by LIMA; bathymetric contour interval of 500 m from IBSCO (Arndt et al., 2013).

4.1.2. Larsen B embayment

Nearly all of the mapped flow indicators in the mid-shelf environment are MSGLs, indicating that ice flowed across this area at a rapid rate. The prevalence of grounding zone features within the Larsen B embayment (Fig. 10) indicates periods of swift deglaciation, punctuated by glacial stillstands (cf., Batchelor and Dowdeswell, 2015).

The CHIRP profiles taken across the Larsen B embayment revealed acoustically chaotic facies, interpreted as till deposits, occasionally overlain by thin acoustically transparent units, interpreted as marine sediment drape. Reconstructed grounding lines in this area were supported not only by multiple grounding zone wedges but also by deeply incised channels mapped on opposing trough walls of Scar Inlet (Fig. 6; the most southern fjord of the Larsen B embayment and site of the remaining Scar Inlet Ice Shelf). These channels suggest high pinning points for the ice within Scar Inlet, forcing meltwater to flow in confined, subglacial channels and support the notion of deglaciation with occasional stillstands. These channels clearly show the orientation of the retreating ice front perpendicular to trough axis within the Scar Inlet (Fig. 10).

4.1.3. Larsen C Ice Shelf system

Grounding zone features are extensive throughout this area, with a primarily northeastern orientation (Fig. 11). They are located parallel to shore, directly mirroring the geography and orientation of the coastline. While there is certainly very little data, the distinct lack of any assemblage other than consistently back-stepped grounding zone features suggests that the Larsen C system may be located in an inter ice stream area, typified by slow or stagnant ice flow. The window of time between pauses in deglacial retreat appears to be shorter in the Larsen C area than in the Larsen A and B embayments. This has led to grounding zone features in the Larsen C system to occur in a more nested distribution (Fig. 11), as more frequent stillstands during less rapid retreat would result in a greater number of closely spaced grounding zone features. This is noted based on distance between each grounding zone feature, as there is no dating available for these wedges. Average distance measured between each successive grounding zone feature (toward the shoreline) in the Larsen C system is 740 m, compared with 1530 m in the Larsen B embayment and 3035 m in the Larsen A embayment.

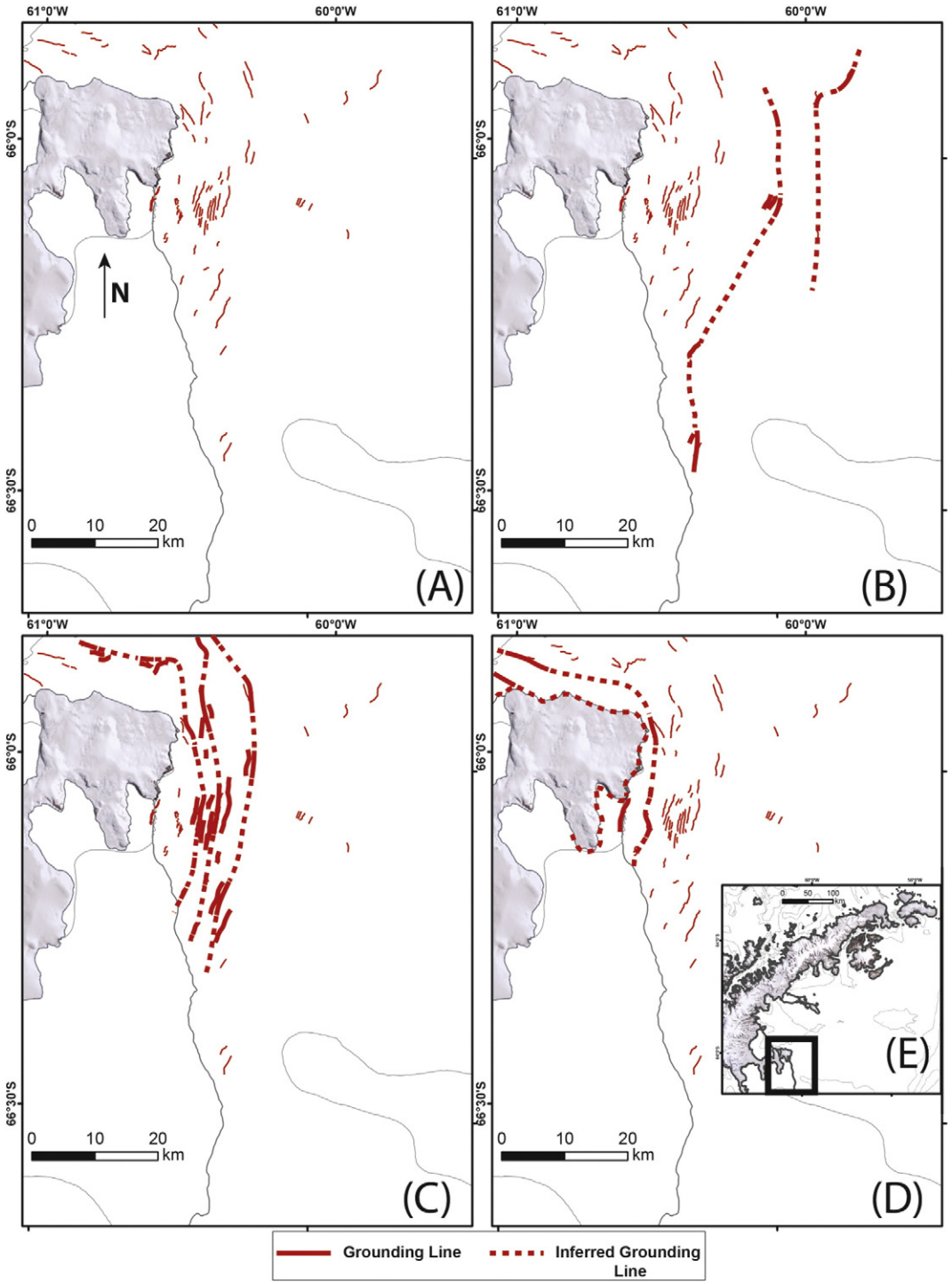

Fig. 11. Grounding line reconstruction for the Larsen C Ice Shelf system. Solid red thin and thick lines indicate mapped grounding zone features; dashed red line indicates inferred grounding zone features. (A) At the LGM, the entire region was covered by grounded ice; (B) early geometry; (C) later geometry; (D) estimated modern day grounding line; (E) location of Larsen C Ice Shelf system on the AP. Background images by LIMA; bathymetric contour interval of 500 m from IBSCO (Arndt et al., 2013).

4.2. Shifting retreat flow patterns

4.2.1. Ice flow on the outer shelf

In Heroy and Anderson, 2007, Heroy and Anderson identified the eastern edge of Robertson Trough as having four generations of cross-cutting MSGL sets. In this study, we identify two primary fabrics instead of four. The additional two cross-cutting fabrics identified in previous studies are actually remarkably parallel iceberg furrows (Fig. 12), originating from the southeast and northeast. There is no third and fourth MSGL flow set in this area, and the second MSGL set is located farther north, out of the path of the parallel iceberg furrows.

The orientation of the iceberg furrows parallel (or very nearly so) to an MSGL flow set (Fig. 12B) suggests the release of very thick, possibly

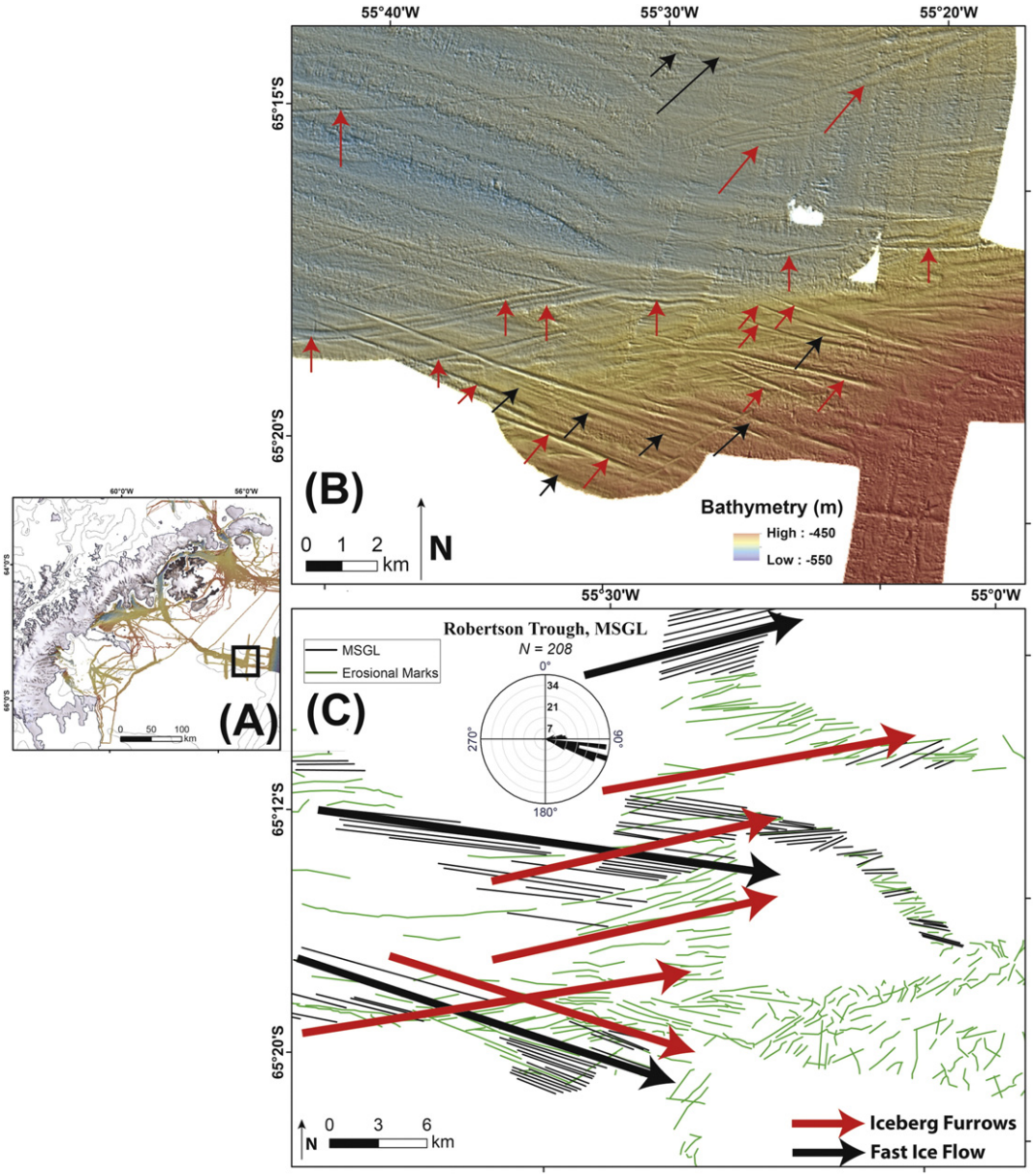

Fig. 12. (A) Location of Robertson Trough in outer shelf area (southeast of James Ross Island and Larsen A embayment). (B) Robertson Trough: MSGL set, oriented southeast (black arrows) cut by iceberg furrows (red arrows). Shading from northeast, no exaggeration. Arrow length is arbitrary. (C) Megascale glacial lineations (thin black lines) and iceberg furrows (thin green lines), overlain by red and black arrows indicating primary directional sets. The iceberg furrow sets include randomly oriented furrows, primarily on the east side of the area shown, and furrows in subparallel sets. Arrow length is arbitrary.

grounded, ice from near the grounding line. This type of massive calving event would produce either a single, deep-keeled iceberg with multiple *bottom bumps* or a pack of deep-keeled icebergs traveling together (an *iceberg armada*), ploughing along the seafloor in the direction of ice streaming (Jakobsson et al., 2011, 2012; López-Martínez et al., 2011). The iceberg ploughmarks in Robertson Trough (Fig. 1) show relatively little of the usual sinuosity and random drag patterns typically expected of such features (Dowdeswell and Bamber, 2007). The iceberg, or iceberg armada, recorded in this study area was transported directly away from a grounding line in the direction of drainage from the active ice stream. Icebergs would probably move to the edge of the trough, where the ice would either ground briefly in the shallower depths or experience breakup and melting as a dispersal mechanism. An alternative interpretation to a sudden release of many icebergs from the grounding line is that the grounding line was at the same position for a long period of time and continuously discharging icebergs at a slow rate. While this is certainly possible, the preservation of MSGLs with approximately the same sediment cover as the iceberg ploughmarks (what originally led to the interpretation as representing many MSGL sets; Heroy and Anderson, 2005), leads to our preferred interpretation of grounding line retreat.

Tidally influenced corrugation ridges noted to be associated with thick packages of released ice, whether single or as an armada (Jakobsson et al., 2011; Andreassen et al., 2014), are not detected in this area. Our data in this part of the study area is vintage, lower-resolution multibeam data that does not resolve small-scale features such as small corrugation ridges; thus, the lack of corrugations in the images may not be indicative of the full set of seafloor

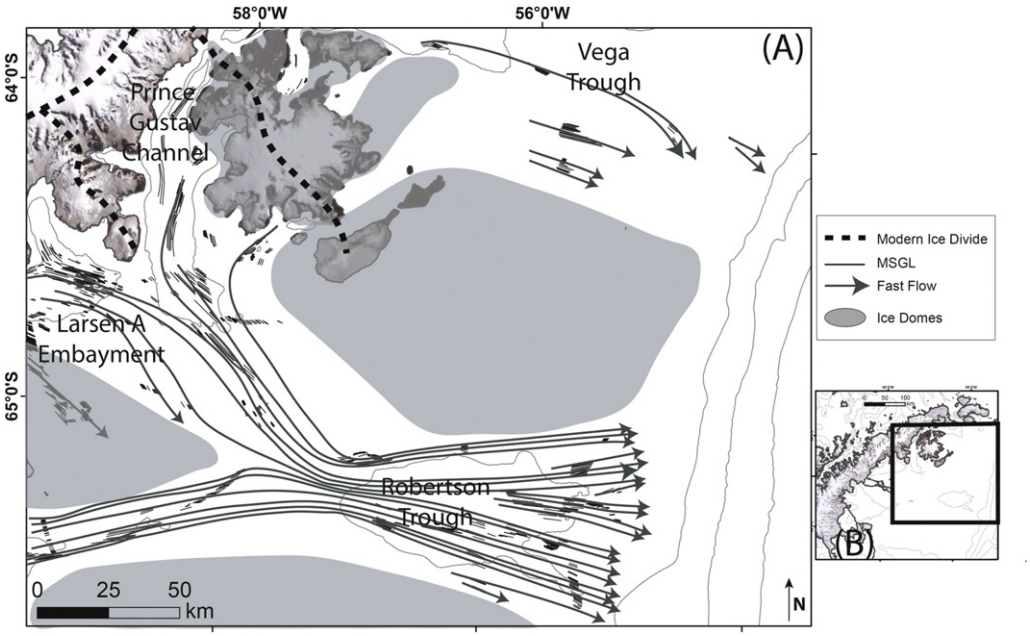

Fig. 13. Northwestern Weddell Sea: (A) ice streaming and flow map with labeled troughs. Gray arrows indicate fast, or streaming, ice flow. Black dashed lines indicate the modern ice divide, gray areas show proposed ice domes (Lavoie et al., 2015); (B) location of outer shelf area on the AP. Bathymetric contour interval of 500 m from IBSCO (Arndt et al., 2013).

features here. Alternatively, corrugation ridges may not have formed in this location if the tidal influence was not significant across the wide, open shelf in this area at the time of calving. A calving event of this size could be related to glacial acceleration caused by the collapse of an ice shelf. Ice flow within the Robertson Trough shows two diverging directions, to the southeast and northeast (Fig. 12C). For the most part, the two flow sets do not interact within the data coverage. Cross-cutting relationships appear to show the northeastern flow set cutting the southeastern set; however, this relationship is tenuous at best, owing to extensive overprinting by iceberg furrows as well as limited data coverage in areas of cross-cutting. It is tentatively suggested that the northeastern flow set postdates the southeastern set, where the two overlap. Final flow assemblages for Robertson Trough are shown in Fig. 12C.

Development of MSGLs is dependent on an adequate sediment supply moving under the ice to generate the features (Clark et al., 2003; Livingstone et al., 2016). The presence of multiple sets of these lineations on the outer shelf shows that sediment is being transported across the shelf, allowing these features to develop. It is unknown from this work how much of the sediment is being transported from the rugged inner shelf and how much is being sourced more locally by erosion of the underlying outer shelf. However, based on the comparatively smooth substrate across the wide outer shelf (Figs. 1 and 12) and the continuous till cover implied by the distribution of MSGLs, it does not seem that ice was eroding into the outer shelf substrate, except underneath a deforming till layer. This suggests a till conveyor belt from the rugged inner shelf, at least as far as the MSGLs have been mapped. The discontinuous nature of our multibeam, largely due to ice cover in the Weddell Sea, does not allow for length measurement of individual MSGLs. However, the distance from a source for till generation (in other words, a long run-out distance) suggests highly elongated features and thus lower shear strengths and higher ice velocities. Jamieson et al. (2016) recently suggested that there is also a correlation between the height of MSGLs and bed strength, with smaller heights representing lower basal shear stress and thus greater ice velocities. This relationship will give a new way to qualitatively assess ice velocities where data sets do not allow more length measurements.

Ice flow in Robertson Trough is directly related to flows emanating from the Larsen A and B embayments and the southern outlet of the Prince Gustav Channel (Fig. 13) and represents the final drainage path of a major ice stream draining the middle section of the study area (Lavoie et al., 2015).

4.2.2. Transient flow paths on the inner shelf

Fig. 14 illustrates the drumlinoid geometry south of Bombardier Bay. This geomorphic expression, which we refer to as nested rock drumlins, does not have a direct or obvious analogue in any other published study from high latitude environments. Compound and fused drumlins have previously been noted in the Omagh Basin in Ireland by Knight (1997); however, these drumlins were confined to higher elevations, whereas the nested rock drumlins in this study are located within a trough. Barchanoid and Y-shaped drumlins with varying degrees of superimposition have also been noted in Canada, Ireland (Clark and Meehan, 2001), and Scotland (Rose and Letzer, 1977) but with different geometries than the nested rock drumlins described here. Subglacial bedforms, particularly drumlins, often form as features in a continuum, falling somewhere between erosional and depositional (Benn and Evans, 1998). Features mapped in Marguerite Bay, West Antarctica, have been termed *whalebacks*, which describe oval-shaped hills that are formed exclusively in bedrock (Livingstone et al., 2013); these features occur as sets with each feature subparallel to its neighbor. Unimodal populations are occasionally noted throughout glacial environments (e.g., Ireland, Canada; Clark and Meehan, 2001); however, the key concept is that ice flow is dynamic, therefore full populations are rarely entirely uniform. The superimposition of the smaller drumlins on top of larger, asymmetric drumlins suggests a dynamic glacial environment that is steadily oscillating, possibly during active movement of the grounding line of the glacier. The confluence of the three active glacial systems within this trough (Fig. 14A) suggests an incomplete erosional smoothing owing to alternations of dominant flow directions. Significant readvance of any of these glacial systems within the trough is not considered likely, based on the absence of any moraines or

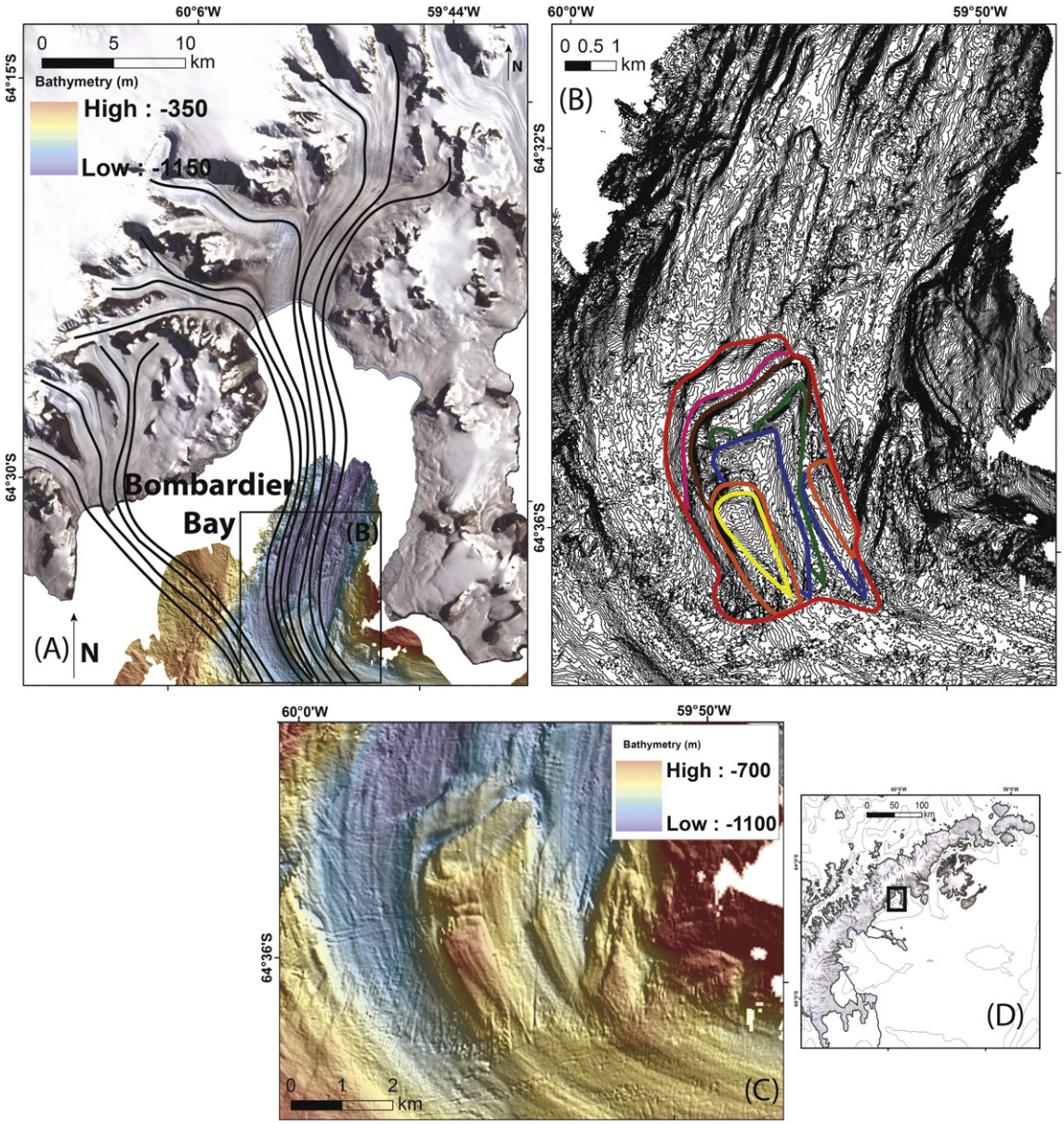

Fig. 14. Bombardier Bay (Larsen A embayment): (A) Shaded bathymetric map, showing confluence of glacial outlet flows (black lines), background image by LIMA; (B) topographic map, contour interval 5 m, showing the successive superimposition of smaller drumlins on initial parent drumlin. Red indicates oldest generation (successively, pink, brown, green, blue, orange, yellow being the youngest); (C) Uninterpreted multibeam image of the nested drumlins, exaggeration of 5, shaded from the northeast; (D) Location of Bombardier Bay on the AP.

grounding zone features within the trough. Subbottom profiles taken over the nested drumlins reveal an acoustically chaotic unit with a strong surface reflector and no sediment classified as crystalline bedrock (seismic facies 6 in Figs. 2 and 15).

The flow patterns that frame the Seal Nunataks (Fig. 16) to the north and south are strongly oriented southeast (Figs. 4 and 5), with a small component of northeasterly flow from the Larsen B that occurs when the two flow sets converge east of Robertson Island (Fig. 5). This similar flow direction and eventual convergence suggests that the mapped MSGLs in the Larsen A and B embayments are possibly related to the same flow event, involving ice streaming from a centralized ice dome or ice domes connected to the primary APIS. This implies that flow communication between Larsen A and B embayments did occur in the past as the result of a shared ice mass.

In the Larsen A embayment, ice stream onset and eventual acceleration is noted in Greenpeace Trough, based on the presence of drumlins that grade in MSGLs. These flow indicators are oriented strongly northeast (Fig. 16). The large series of glacial grooves at the ice shelf edge of the Seal Nunataks are also strongly oriented northeast and appear to be coincident with the onset of ice streaming in Greenpeace Trough. These grooves share the same orientation with the smaller rock drumlins mapped in the coastal area of the Seal Nunataks. This suggests that an early ice stream, at or near the LGM, was flowing over the Seal Nunataks into Greenpeace Trough. The first stage of flow is shown by pink arrows in Fig. 16. The second flow pattern, originating from reorientation of the changing ice dome geometry, is shown in green arrows.

The curvilinear glacial flutings present in the northern side of the Seal Nunataks deviate from the northeastern flow directions shown

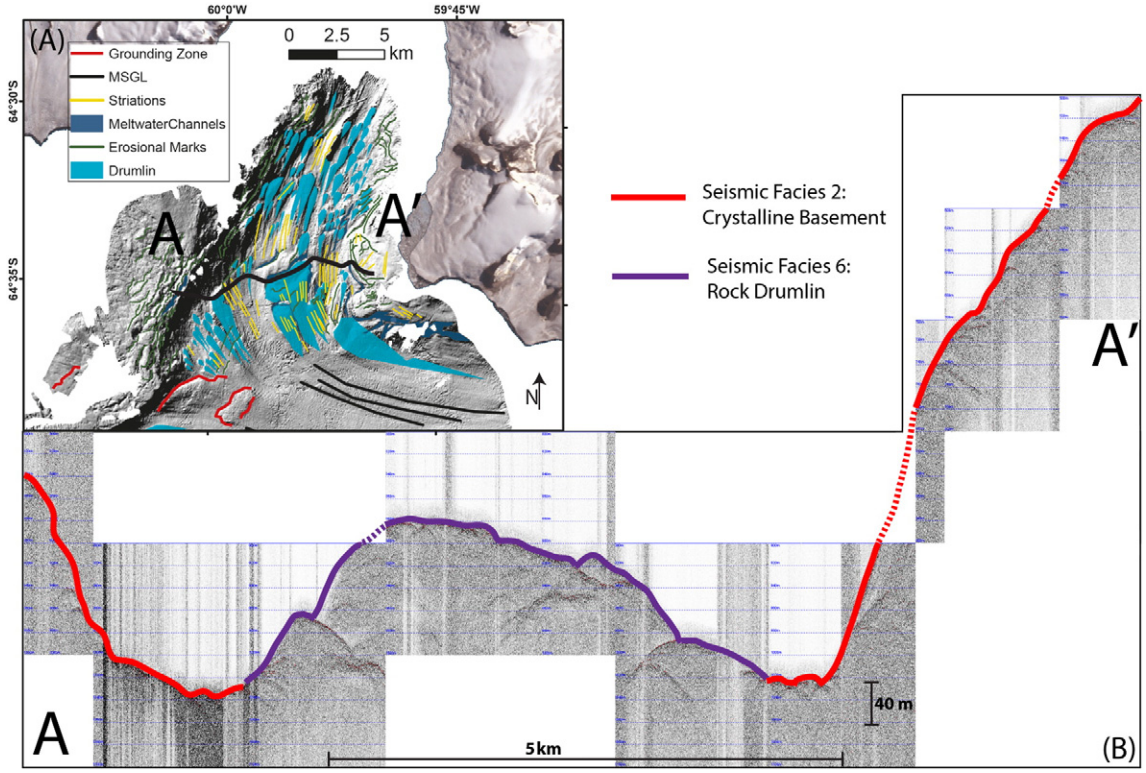

Fig. 15. Bombardier Bay (Larsen A embayment): (A) Shaded relief map, showing subbottom profiles line A–A′; (B) interpreted subbottom profile A–A′, vertical exaggeration is 48:1.

by the grooves, drumlins, and MSGLs in the Larsen A embayment. Morphologically, they are similar to the adjacent flow set of MSGLs; however, their curved trajectory precludes their classification as true MSGLs. Bathymetric profiles taken over the features show positive topography (Fig. 17), indicating depositional origin, which supports our assertion of these as glacial lineations. The included CHIRP profile over A to A′ (Fig. 17) shows positive features belonging to seismic facies 3, which indicates subglacial till. They represent

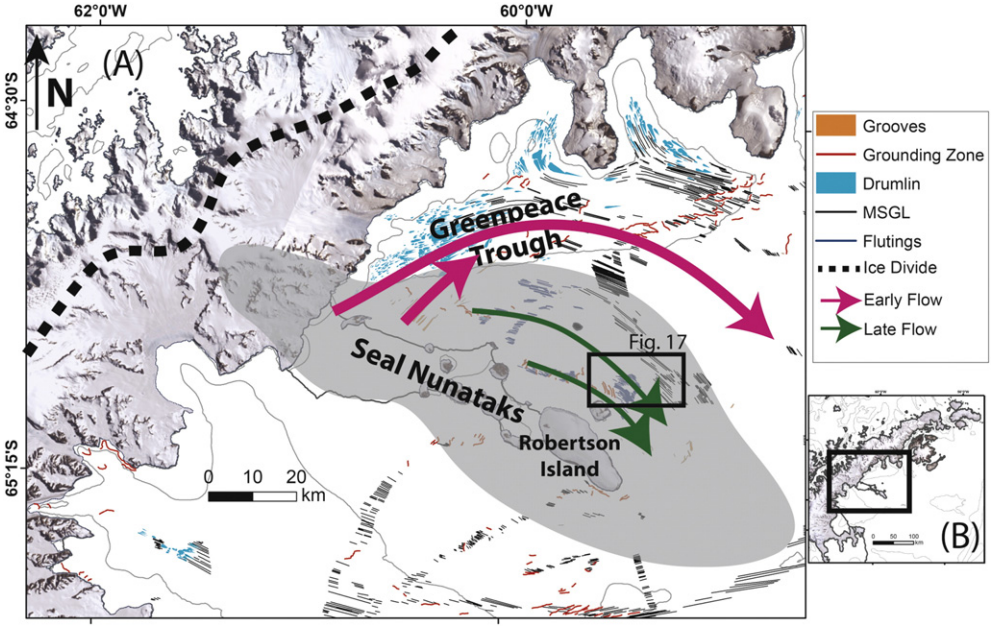

Fig. 16. Two stages of flow are shown for the Larsen A and B embayments. (A) Early (LGM) flow patterns for Larsen A and B embayments (pink arrows) during a period in which ice covered the study area. Later flow (green arrows) shows reorientation of ice flow underneath Robertson Ice Dome. Black box denotes location of Fig. 16. Mapped flow indicators are shown, black dashed lines indicate the modern ice divide, gray areas show proposed ice domes (Lavoie et al., 2015). (B) Location of Seal Nunataks on the AP. Background images by LIMA; bathymetric contour interval of 500 m from IBSCO (Arndt et al., 2013).

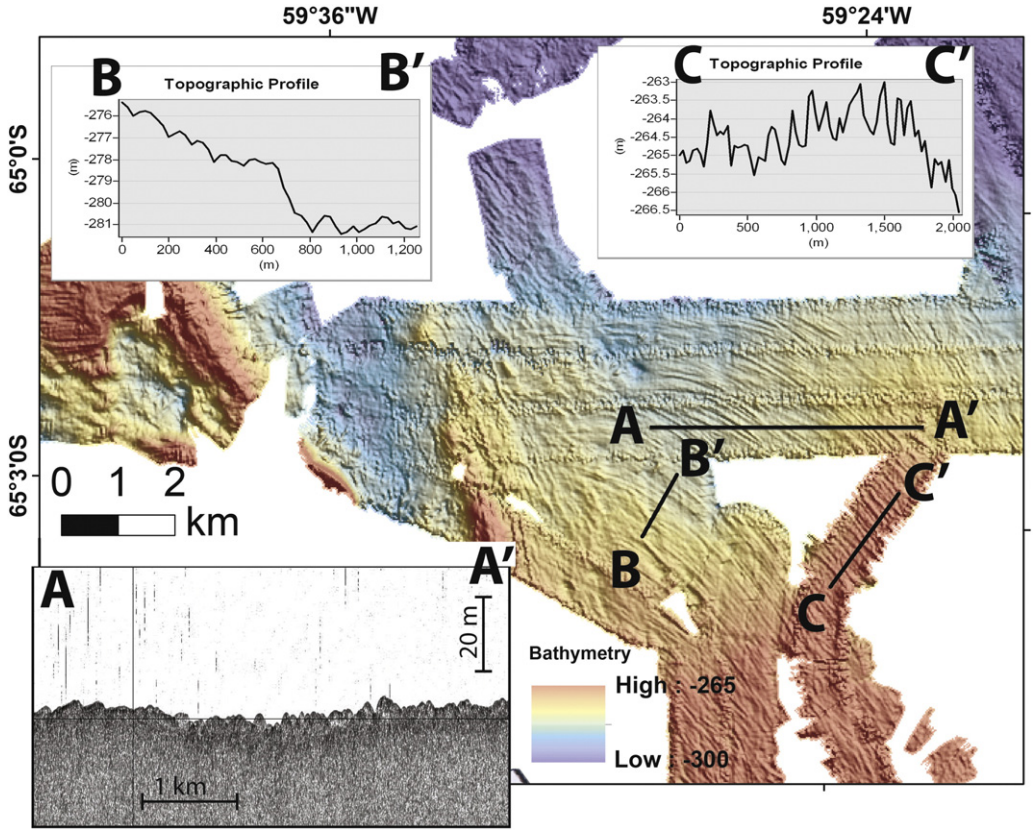

Fig. 17. CHIRP subbottom profile (A–A′) and topographic profiles (B–B′, C–C′) located on map drawn over selected surveyed areas adjacent to the Seal Nunataks. Shapes of features resolved in the profiles indicate depositional geomorphic bedforms, as seen by positive amplitudes, with no suggestive geometries of morainal features.

drainage from the Robertson Dome but cannot be interpreted to represent fast or streaming flow. Their proximity to the northeastern flow sets suggests that these glacial flutings are representative of a different flow orientation. Their slower, more southeasterly, flow pattern is suggested to show a later stage of flow, as the Robertson Ice Dome and AP Ice Sheet shrank toward the coastline during deglaciation. The recession of the ice toward the Seal Nunataks concentrated the slower ice flow northeast of the dome in a primarily southeastern pattern, as evidenced by the flutings. This later stage of flow is represented by the green arrows in Fig. 16. The glacial flutings noted in the Seal Nunataks were considered as possible morainal features, such as ringed moraines, which may have encircled the previous ice dome at each stage of its deglacial stillstands. However, the lack of continued features, which would be expected of ringed moraines, south and southwest of the Seal Nunataks does not support this hypothesis. While any deglacial features off the most southeastern tip of Robertson Island (the most seaward of the Seal Nunataks) are all but completely obliterated by massive iceberg ploughmarks, multibeam data in the Larsen B embayment would show geometric alignment in such close proximity to the Seal Nunataks were there to be any encircling, ringed moraines. No such features could be found.

4.3. Shelf geomorphology

The submarine glacial geomorphology of the northeastern AP is an isolated, characteristic reflection of the specific glacial environment that sources it. While all glacial environments are inherently different, the ice-sculpted or -eroded features exhibit characteristics across a continuous spectrum as a result of the shared origin. Measured features in this study have been compared to different glacial environments including drumlins (Rõuk and Raukas, 1989; Knight, 1997; Evans et al., 2004; Briner, 2007; Ottesen et al., 2008; Clark et al., 2009; Graham et al., 2009; Ottesen and Dowdeswell, 2009; Batchelor et al., 2011; Robinson and Dowdeswell, 2011; Lamsters, 2012) and megascale glacial lineations (Ó Cofaigh et al., 2002; Andreassen et al., 2004, Andreassen et al., 2008; Graham et al., 2007, Graham et al., 2009; Ottesen et al., 2008; Clark et al., 2009; Greenwood and Kleman, 2010; Rebesco et al., 2011; Robinson and Dowdeswell, 2011; Stokes et al., 2013; Spagnolo, et al. 2014) from a variety of settings (Figs. 18 and 19). Graphical comparisons were constructed, and we present here that the drumlins in the eastern AP are among the largest features mapped in published glacial studies (Fig. 18). Large features that have similar geometries do exist on the Antarctic shelf, including in the Amundsen Sea (e.g., Larter et al., 2009; Nitsche et al., 2013), Marguerite Bay (Livingstone et al., 2016), the Gerlache Straight (Evans et al., 2004), and offshore East Antarctica (McMullen et al., 2006); however, their large size often means that they are incompletely imaged or that there are just a few of them, making statistics at this end of the size range difficult. It is clear that drumlins have now been described in most drainage outlets and at wide range of scales. Graphical results for the MSGLs are not presented because these features are often mapped only as a minimum because of incomplete multibeam coverage.

Morphometric measurements show that drumlins in the eastern AP have generally higher widths and lengths than drumlins mapped in similar glacial areas (i.e., marine terminating ice sheets). Elongation ratios for drumlins and MSGLs in the eastern AP are comparatively high, as seen in the graphical analysis of Fig. 19.

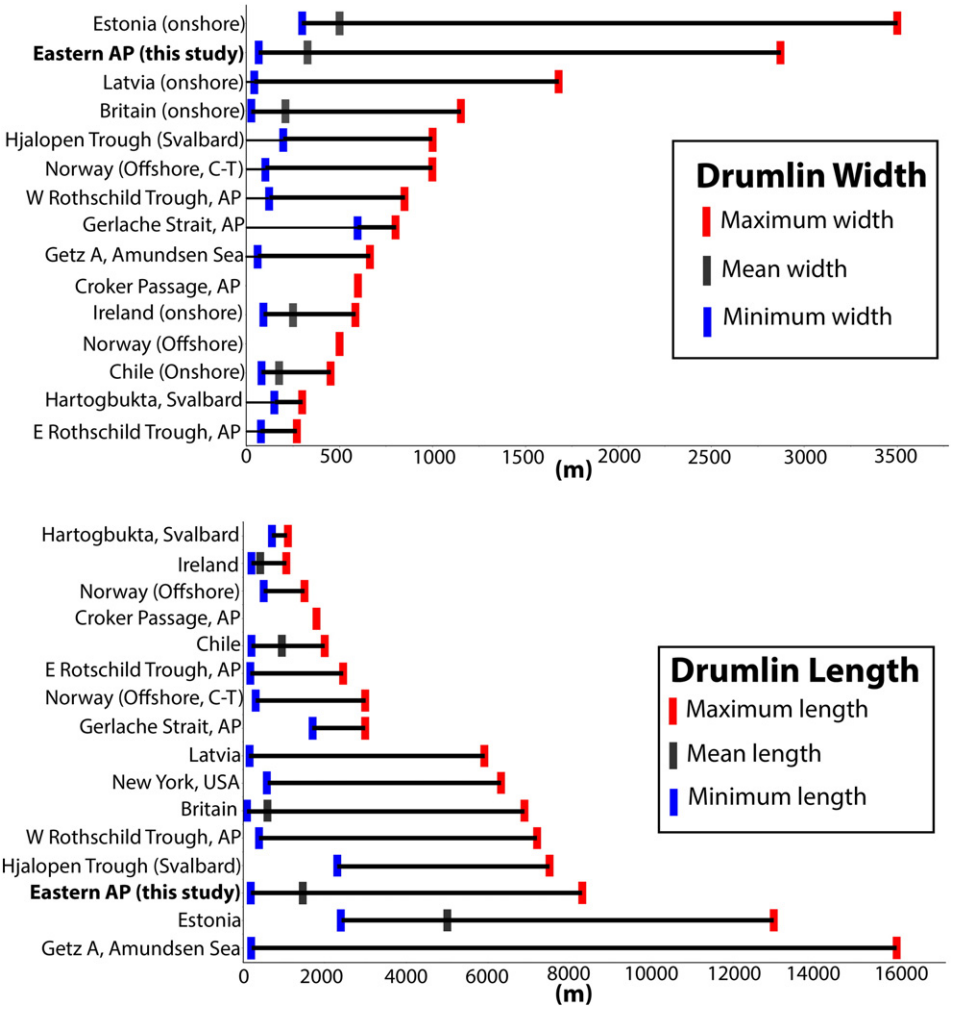

Fig. 18. (Top) Drumlin morphometric width measurements, in m; (Bottom) drumlin morphometric length measurements, in m.

Higher elongation ratios correspond to faster ice flow in the case of MSGLs, which suggests that the style of ice streaming in the eastern AP is faster than in many similar glacial landscapes. Larger drumlins with higher degrees of streamlining may be reflective of a thicker ice sheet acting on a thicker package of dilatant, deformation till (Fowler, 2010). While drumlins are considered to form in the onset zone of ice stream acceleration, the high degree of streamlining in this area implies ongoing rapid flow coupled to the seafloor as ice continued to flow offshore.

5. Conclusions

A major paleo-ice stream and its associated geomorphic assemblages, including those previously designated the Robertson Ice Stream, was mapped in this study, confirming several previous identifications (Evans et al., 2005; Johnson et al., 2011; Davies et al., 2012a,b; Ó Cofaigh et al., 2014; Lavoie et al., 2015). Across the eastern AP, it is likely that at least two major paleo-ice streams were in operation at some point in time during the LGM. Episodic deglacial histories affected the entire study area. The high elongation ratios calculated for drumlins and MSGLs in the eastern AP suggests that ice flowed very rapidly in the eastern AP during deglaciation. We have shown transient flow directions over the Seal Nunataks and emptying into the Larsen A embayment, with one significant reorientation of flow during the deglacial history. This suggests that ice flowed through the topographic divide of the Seal Nunataks from the south. Iceberg activity parallel to flow has been noted within Robertson Trough. This identifies a major calving event at the grounding line of the APIS, likely attributable to the loss of an ice shelf. The location and mapping of grounding zones indicates an episodic deglacial history across the continental shelf. The ice sheet retreated more swiftly within topographically controlled troughs and remained pinned on the high points. Additional flow reorganization during grounding line retreat and thinning of the ice cover are indicated by multiple directions of MSGL on the outer shelf and by cross-cutting relationships in the newly acquired Larsen C data. This mapping indicates the flow reorganization that took place as ice retreated from the outer shelf into the mouth of the more topographically variable inner shelf. The retreat history preserved in geomorphic details described here records varying flow conditions as the grounding line moved back across the shelf. These details can be used as constraints in models of past ice flow and thus help better tune models of future ice behavior.

Acknowledgements

We thank the science parties and captains and crews of each of the cruises that have collected the data used in this paper, particularly KOPRI cruise ARA1304, funded by PP16010. Special thanks to Paul Morin and the Polar Geospatial Center for their exceptional GIS catalogue of Antarctic data sets. This work was funded by NSF 0732614.

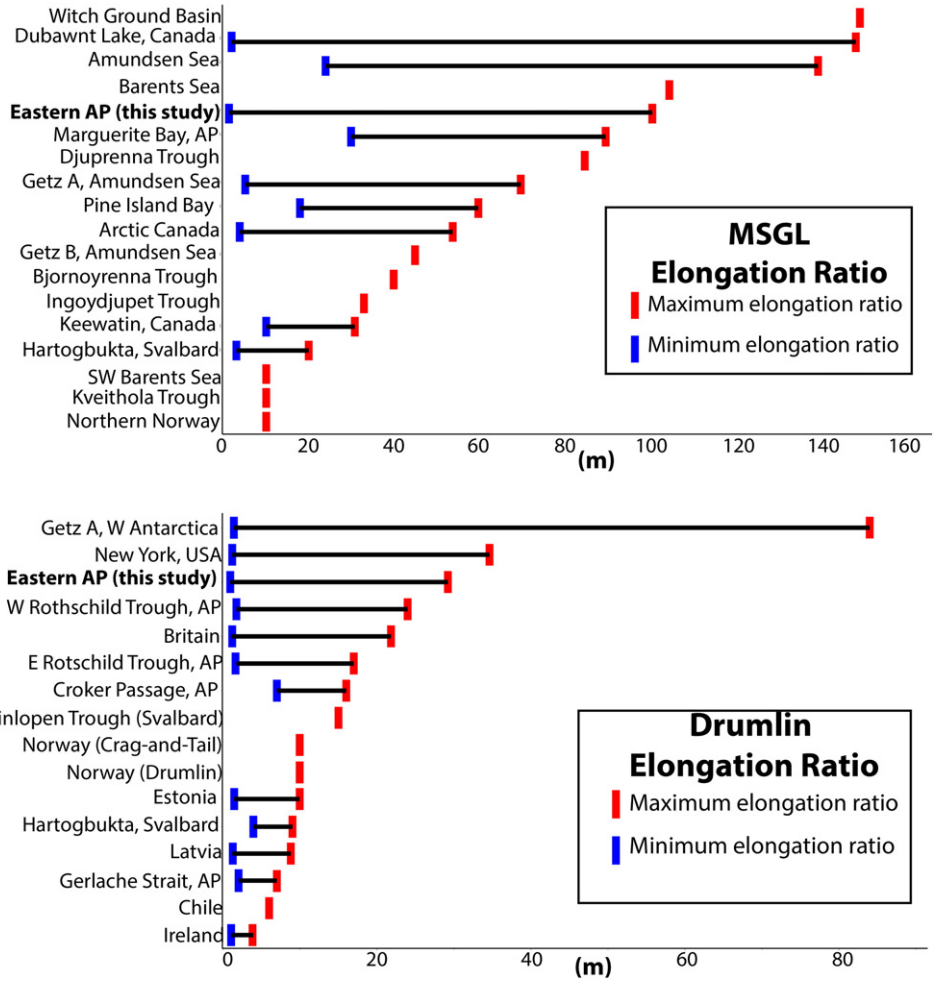

Fig. 19. (Top) MSGL elongation ratios; (Bottom) drumlin elongation ratios.

References

Anderson, J.B., Wellner, J.S., Lowe, A.L., Mosola, A.B., Shipp, S.S., 2001. Footprint of the expanded West Antarctic Ice Sheet: ice stream history and behavior. Geology 11, 4–9.

Anderson, J.B., Shipp, S.S., Lowe, A.L., Wellner, J.S., Mosola, A.B., 2002. The Antarctic Ice Sheet during the Last Glacial Maximum and its subsequent retreat history: a review. Quat. Sci. Rev. 21, 49–70.

Andreassen, K., Nilssen, L.C., Rafaelsen, B., Kuilman, L., 2004. Three-dimensional seismic data from the Barents Sea margin reveal evidence of past ice streams and their dynamics. Geology 32 (8), 729–732.

Andreassen, K., Laberg, J.S., Vorren, T.O., 2008. Seafloor geomorphology of the SW Barents Sea and its glaci-dynamic implications. Geomorphology 97 (1), 157–177.

Andreassen, K., Winsborrow, M., Bjarnadottir, L.R., Rüther, D.C., 2014. Ice stream retreat dynamics inferred from an assemblage of landforms in the northern Barents Sea. Quat. Sci. Rev. 92, 246–257.

Arndt, J.E., Schenke, H.W., Jakobsson, M., Nitsche, F.O., Buys, G., Goleby, B., Rebesco, M., Bohoyo, F., Hong, J., Black, J., Greku, R., Udintsev, G., Barrios, F., Reynoso-Peralta, W., Taisei, M., Wigley, R., 2013. The International Bathymetric Chart of the Southern Ocean (IBCSO) version 1.0 - a new bathymetric compilation covering circum-Antarctic waters. Geophys. Res. Lett. 40, 3111–3117.

Batchelor, C.L., Dowdeswell, J.A., 2015. Ice-sheet grounding-zone wedges (GZWs) on high-latitude continental margins. Mar. Geol. 363, 65–92.

Batchelor, C.L., Dowdeswell, J.A., Hogan, K.A., 2011. Late Quaternary ice flow and sediment delivery through Hinlopen Trough, Northern Svalbard margin: submarine landforms and depositional fan. Mar. Geol. 284 (1), 13–27.

Benn, D.I., Evans, D.J.A., 1998. Glaciers and Glaciation. second ed. Routledge, New York (784 pp.).

Bentley, M.J., 1999. Volume of Antarctic Ice at the Last Glacial Maximum and its impact on global sea level change. Quat. Sci. Rev. 18, 1569–1595.

Brachfeld, S., Domack, E., Kissel, C., Laj, C., Leventer, A., Ishman, S., Gilbert, R., Camerlenghi, A., Eglinton, L.B., 2003. Holocene history of the Larsen-A Ice Shelf constrained by geomagnetic paleointensity dating. Geology 31 (9), 749–752.

Briner, J.P., 2007. Supporting evidence from the New York drumlin field that elongate subglacial bedforms indicate fast flow. Boreas 36, 143–147.

Camerlenghi, A., Domack, E., Rebesco, R., Gilbert, R., Ishman, S., Leventer, A., Brachfeld, S., Drake, A., 2001. Glacial morphology and post-glacial contourites in northern Prince Gustav Channel (NW Weddell Sea, Antarctica). Mar. Geophys. Res 22, 417–443.

Canals, M., Urgeles, R., Calafat, A., 2000. Deep sea-floor evidence of past ice streams off the Antarctic Peninsula. Geology 28, 31–34.

Clark, C.D., 1993. Mega-scale glacial lineations and cross-cutting ice-flow landforms. Earth Surf. Process. Landf. 18, 1–29.

Clark, C.D., Meehan, R.T., 2001. Subglacial bedform geomorphology of the Irish Ice Sheet reveals major configuration changes during growth and decay. J. Quat. Sci. 16 (5), 483–496.

Clark, C.D., Tulaczyk, S.M., Stokes, C.R., Canals, M., 2003. A groove-ploughing theory for the production of mega-scale glacial lineations, and implications for ice-stream mechanics. J. Glaciol. 49 (165), 240–256.

Clark, C.D., Hughes, A.L.C., Greenwood, S.L., Spagnolo, M., Ng, F.S.L., 2009. Size and shape characteristics of drumlins, derived from a large sample and associated scaling laws. Quat. Sci. Rev. 28, 677–692.

Davies, B.J., Hambrey, M.J., Smellie, J.L., Carravick, J.L., Glasser, N.F., 2012a. Antarctic Peninsula Ice Sheet evolution during the Cenozoic Era. Quat. Sci. Rev. 31:30–66. http://dx.doi.org/10.1016/j.quascirev.2011.10.012.

Davies, B.J., Carravick, J.L., Glasser, N.F., Hambrey, M.J., Smellie, J.L., 2012b. Variable glacier response to atmospheric warming, northern Antarctic Peninsula, 1988–2009. Cryosphere 6:1031–1048. http://dx.doi.org/10.5194/tc-6-1031-2012.

Domack, E., Duran, D., Leventer, A., Ishman, S., Doane, S., McCallum, S., Amblas, D., Ring, J., Gilbert, R., Prentice, M., 2005. Stability of the Larsen B Ice Shelf on the Antarctic Peninsula during the Holocene epoch. Nature 436, 681–685.

Domack, E., Amblàs, D., Gilbert, R., Brachfeld, S., Camerlenghi, A., Rebesco, M., Canals, M., Urgeles, R., 2006. Subglacial morphogy and glacial evolution of the Palmer deep outlet system, Antarctic Peninsula. Geomorphology 75, 125–142.

Domack, E., Leventer, A., Gilbert, R., Brachfeld, S., Ishman, S., Camerlenghi, A., Gavahan, K., Carlson, D., Barkoukis, A., 2001. Cruise reveals history of Holocene Larsen Ice Shelf. Eos Trans. AGU 82 (2), 13–17.

Dowdeswell, J.A., Bamber, J.L., 2007. Keel depths of modern Antarctic icebergs and implications for sea-floor scouring in the geological record. Mar. Geol. 243, 120–131.

Dowdeswell, J.A., Ó Cofaigh, C., Pudsey, C.J., 2004. Continental slope morphology and sedimentary processes at the mouth of an Antarctic palaeo-ice stream. Mar. Geol. 204, 203–214.
Evans, J., Dowdeswell, J.A., Ó Cofaigh, C., 2004. Late Quaternary submarine bedforms and ice-sheet flow in Gerlache Strait and on the adjacent continental shelf, Antarctic Peninsula. J. Quat. Sci. 19 (4), 397–407.
Evans, J., Pudsey, C.J., Ó Cofaigh, C., Morris, P., Domack, E., 2005. Late Quaternary glacial history, flow dynamics and sedimentation along the eastern margin of the Antarctic Peninsula Ice Sheet. Quat. Sci. Rev. 24, 741–774.
Fowler, A.C., 2010. The formation of subglacial streams and mega-scale glacial lineations. Proc. R. Soc. Lond. Ser. A 466 (2121), 2673–2694.
Fretwell, P., Pritchard, H.D., Vaughan, D.G., Bamber, J.L., Barrand, N.E., Bell, R., Bianchi, C., Bingham, R.G., Blankenship, D.D., Casassa, G., Catania, G., Callens, D., Conway, H., Cook, A.J., Corr, H.F.J., Damaske, D., Damm, V., Ferraccioli, F., Forsberg, R., Fujita, S., Gim, Y., Gogineni, P., Griggs, J.A., Hindmarsh, R.C.A., Holmlund, P., Holt, J.W., Jacobel, R.W., Jenkins, A., Jokat, W., Jordan, T., King, E.C., 2013. Bedmap2: improved ice bed, surface and thickness datasets for Antarctica. Cryosphere 7 (1). http://dx.doi.org/10.5194/tc-7-375-2013.
Gilbert, R., Domack, E., Camerlenghi, A., 2003. Deglacial history of the Greenpeace Trough: ice sheet to shelf transition in the Northwestern Weddell Sea. Antarct. Res. Ser. 79, 195–204.
Glasser, N.F., Davies, B.J., Carrivick, J.L., Rodés, A., Hambrey, M.J., Smellie, J.L., Domack, E., 2014. Ice-stream initiation, duration and thinning on James Ross Island, northern Antarctic Peninsula. Quat. Sci. Rev. 86, 78–88.
Golledge, N.R., Levy, R.H., McKay, R.M., Fogwill, C.J., White, D.A., Graham, A.G., Smith, J.A., Hillenbrand, C.-D., Licht, K.J., Denton, G.H., Ackert Jr., R.P., Mass, S.M., Hall, B.L., 2013. Glaciology and geological signature of the Last Glacial Maximum Antarctic Ice Sheet. Quat. Sci. Rev. 78, 225–247.
Graham, A.G.C., Lonergan, L., Stoker, M.S., 2007. Evidence for Late Pleistocene ice stream activity in the Witch Ground Basin, central North Sea, from 3D seismic reflection data. Quat. Sci. Rev. 26 (5), 627–643.
Graham, A.G.C., Larter, R.D., Gohl, K., Hillenbrand, C., Smith, J.A., Kuhn, G., 2009. Bedform signature of a West Antarctic palaeo-ice stream reveals a multi-temporal record of flow and substrate control. Quat. Sci. Rev. 28, 2774–2793.
Greenwood, S.L., Kleman, J., 2010. Glacial landforms of extreme size in the Keewatin sector of the Laurentide Ice Sheet. Quat. Sci. Rev. 29 (15), 1894–1910.
Grosvenor, D.P., King, J.C., Choularton, T.W., Lachlan-Cope, T., 2014. Downslope föhn winds over the Antarctic Peninsula and their effect on the Larsen Ice Shelves. Atmos. Chem. Phys. 14 (18), 9481–9509.
Heroy, D.C., Anderson, J.B., 2005. Ice-sheet extent of the Antarctic Peninsula region during the Last Glacial Maximum (LGM) – insights from glacial geomorphology. Geol. Soc. Am. Bull. 117 (11–12), 1497–1512.
Heroy, D.C., Anderson, J.B., 2007. Radiocarbon constraints on Antarctic Peninsula Ice Sheet retreat following the Last Glacial Maximum. Quat. Sci. Rev. 26:3286–3297. http://dx.doi.org/10.1016/j.quascirev.2007.07.021.
Jakobsson, M., Anderson, J.B., Nitsche, F.O., Dowdeswll, J.A., Gyllencreutz, R., Kirchner, N., Mohammad, R., O'Rgan, M., Alley, R.B., Anadakrishnan, S., Eriksson, B., Kirshner, A., Fernandez, R., Stolldorf, T., Minzoni, R., Majewski, W., 2011. Geological record of ice shelf break-up and grounding line retreat, Pine Island Bay, West Antarctica. Geology 39:691–694. http://dx.doi.org/10.1130/G32153.1.
Jakobsson, M., Anderson, J.B., Nitsche, F.O., Gyllencreutz, R., Kirshner, A.E., Kirchner, N., O'Regan, M., Mohammad, R., Eriksson, B., 2012. Ice sheet retreat dynamics inferred from glacial morphology of the central Pine Island Bay Trough, West Antarctica. Quat. Sci. Rev. 38, 1–10.
Jamieson, S.S., Stokes, C.R., Livingstone, S.J., Vieli, A., Ó Cofaigh, C., Hillenbrand, C.-D., Spagnolo, M., 2016. Subglacial processes on an Antarctic ice stream bed. 2: can modelled ice dynamics explain the morphology of mega-scale glacial lineations? J. Glaciol. http://dx.doi.org/10.1017/jog.2016.19.
Johnson, J.S., Bentley, M.J., Roberts, S.J., Binnie, S.A., Freeman, S.P., 2011. Holocene deglacial history of the Northeast Antarctic Peninsula–a review and new chronological constraints. Quat. Sci. Rev. 30 (27), 3791–3802.
King, E.C., Woodward, J., Smith, A.M., 2007. Seismic and radar observations of subglacial bedforms beneath the onset zone of Rutford Ice Stream, Antarctica. J. Glaciol. 53 (183), 665–672.
Klages, J.P., Kuhn, G., Graham, A.G.C., Hillenbrand, C.-D., Smith, J.A., Nitsche, F.O., Larter, R.D., Gohl, K., 2015. Palaeo-ice stream pathways and retreat style in the easternmost Amundsen Sea embayment, West Antarctica, revealed by combined multibeam bathymetric and seismic data. Geomorphology 245, 207–222.
Knight, J., 1997. Morphological and morphometric analyses of drumlin bedforms in the Omagh Basin, north central Ireland, Geografiska Annaler: series A. Phys. Geogr. 79 (4), 255–266.
Lamsters, K., 2012. Drumlins and related glaciogenic landforms of the Madliena Tilted Plain, Central Latvian Lowland. Bull. Geol. Soc. Finl. 84 (1), 45–57.
Larter, R.D., Graham, A.G., Gohl, K., Kuhn, G., Hillenbrand, C.D., Smith, J.A., Deen, T.J., Livermore, R.A., Schenke, H.-W., 2009. Subglacial bedforms reveal complex basal regime in a zone of paleo–ice stream convergence, Amundsen Sea embayment, West Antarctica. Geology 37 (5), 411–414.
Lavoie, C., Domack, E.W., Pettit, E.C., Scambos, T.A., Larter, R.D., Schenke, H.W., Yoo, K.C., Gutt, J., Wellner, J., Canals, M., Anderson, J.B., Amblas, D., 2015. Configuration of the Northern Antarctic Peninsula Ice Sheet based upon a new synthesis of seabed imagery. Cryosphere 9, 613–629.
Livingstone, S.J., Ó Cofaigh, C., Stokes, C.R., Hillenbrand, C.-D., Vieli, A., Jamieson, S.S., 2013. Glacial geomorphology of Marguerite Bay palaeo-ice stream, western Antarctic Peninsula. J. Maps 9 (4), 558–572.
Livingstone, S.J., Stokes, C.R., Ó Cofaigh, C., Hillenbrand, C.D., Vieli, A., Jamieson, S.S., Spagnolo, M., Dowdeswell, J.A., 2016. Subglacial processes on an Antarctic ice stream bed. 1: sediment transport and bedform genesis inferred from marine geophysical data. J. Glaciol. 62 (232), 270–284.
López-Martínez, J., Muñoz, J.A., Dowdeswell, C.L., Acosta, J., 2011. Relict sea-floor ploughmarks record deep-keeled Antarctic icebergs to 45° S on the Argentine margin. Mar. Geol. 288 (1), 43–48.
McMullen, K., Domack, E., Leventer, A., Olson, C., Dunbar, R., Brachfeld, S., 2006. Glacial morphology and sediment formation in the Mertz Trough, East Antarctica. Palaeogeogr. Palaeoclimatol. Palaeoecol. 231 (1), 169–180.
Nitsche, F.O., Gohl, K., Larter, R.D., Hillenbrand, C.-D., Kuhn, G., Smith, J.A., Jacobs, S., Anderson, J.B., Jakobsson, M., 2013. Paleo ice flow and subglacial meltwater dynamics in Pine Island Bay, West Antarctica. Cryosphere 7 (1), 249–262.
Nývlt, D., Braucher, R., Engel, Z., Mlčoch, B., Team, A.S.T.E.R., 2014. Timing of the Northern Prince Gustav Ice Stream retreat and the deglaciation of northern James Ross Island, Antarctic Peninsula during the last glacial–interglacial transition. Quat. Res. 82 (2), 441–449.
Ó Cofaigh, C., Pudsey, C.J., Dowdeswell, J.A., Morris, P., 2002. Evolution of subglacial bedforms along a paleo-ice stream, Antarctic Peninsula continental shelf. Geophys. Res. Lett. 29 (8):41-1–41-4. http://dx.doi.org/10.1029/2001GL014488.
Ó Cofaigh, C., Dowdeswell, J.A., Allen, C.S., Hiemstra, J.F., Pudsey, C.J., Evans, J., Evans, D.J., 2005. Flow dynamics and till genesis associated with a marine-based Antarctic palaeo-ice stream. Quat. Sci. Rev. 24 (5), 709–740.
Ó Cofaigh, C., Davies, B.J., Livingstone, S.J., Smith, J.A., Johnson, J.S., Hocking, E.P., Hodgson, D.A., Anderson, J.B., Bentley, M.J., Canals, M., Domack, E., Dowdeswell, J.A., Evans, J., Glasser, N.F., Hillenbrand, C.D., Larter, R.D., Roberts, S.J., Simms, A.R., 2014. Reconstruction of ice-sheet changes in the Antarctic Peninsula since the Last Glacial Maximum. Quat. Sci. Rev. 100, 87–110.
Ottesen, D., Dowdeswell, J., 2009. An inter-ice-stream glaciated margin: submarine landforms and geomorphic model based on marine geophysical data from Svalbard. Geol. Soc. Am. Bull. 121 (11–12), 1647–1665.
Ottesen, D., Stokes, C.R., Rise, L., Olsen, L., 2008. Ice-sheet dynamics and ice streaming along the coastal parts of northern Norway. Quat. Sci. Rev. 27 (9), 922–940.
Pudsey, C.J., 2000. Sedimentation on the continental rise west of the Antarctic Peninsula over the last three glacial cycles. Mar. Geol. 167 (3), 313–338.
Rebesco, M., Liu, Y., Camerlenghi, A., Winsborrow, M., Laberg, J.S., Caburlotto, A., Diviacco, P., Accettella, D., Sauli, C., Wardell, N., Tomini, I., 2011. Deglaciation of the western margin of the Barents Sea Ice Sheet – a swath bathymetric and subbottom seismic study from the Kveithola Trough. Mar. Geol. 279 (1), 141–147.
Rebesco, M., Domack, E., Zgur, F., Lavoie, C., Leventer, A., Brachfeld, S., Willmott, V., Halverson, G., Truffer, M., Scambos, T., Smith, J., Pettit, E., 2014. Boundary condition of grounding lines prior to collapse, Larsen-B Ice Shelf, Antarctica. Science 345, 1354–1358.
Robinson, P., Dowdeswell, J.A., 2011. Submarine landforms and the behavior of a surging ice cap since the Last Glacial Maximum: the open-marine setting of eastern Austfonna, Svalbard. Mar. Geol. 286 (1), 82–94.
Rose, J., Letzer, J.M., 1977. Superimposed drumlins. J. Glaciol. 18 (80), 471–480.
Rõuk, A.-M., Raukas, A., 1989. Drumlins of Estonia. Sediment. Geol. 62, 371–384.
Shipp, S.S., Wellner, J.S., Anderson, J.B., 2002. Retreat signature of a polar ice stream: subglacial geomorphic features and sediments from the Ross Sea, Antarctica. Geol. Soc. Lond., Spec. Publ. 203 (1), 277–304.
Spagnolo, M., Clark, C.D., Ely, J.C., Stokes, C.R., Anderson, J.B., Andreasson, K., Graham, A.G.C., King, E.C., 2014. Size, shape, and spatial arrangement of mega-scale glacial lineations from a large and diverse dataset. Earth Surf. Process. Landf. 39, 1432–1448.
Spagnolo, M., Phillips, E., Piotrowski, J.A., Rea, B.R., Clark, C.D., Stokes, C.R., Carr, S.J., Ely, J.C., Ribolini, A., Wysota, W., Szuman, I., 2016. Ice stream motion facilitated by a shallow-deforming and accreting bed. Nat. Commun. http://dx.doi.org/10.1038/ncomms10723.
Stokes, C.R., Clark, C.D., 2002. Are long subglacial bedforms indicative of fast ice flow? Boreas 31 (3), 239–249.
Stokes, C.R., Fowler, A.C., Clark, C.D., Hindmarsh, R.C.A., Spagnolo, M., 2013. The instability theory of drumlin formation and its explanation of their varied composition and internal structure. Quat. Sci. Rev. 62, 77–96.
Vaughan, D.G., Marshall, G.J., Connolley, W.M., Parkinson, C., Mulvaney, R., Hodgson, D.A., King, J.C., Pudsey, C.J., Turner, J., 2003. Recent rapid regional climate warming of the Antarctic Peninsula. Clim. Chang. 60, 243–274.
Wellner, J.S., Lowe, A.L., Shipp, S.S., Anderson, J.B., 2001. Distribution of glacial geomorphic features on the Antarctic continental shelf and correlation with substrate: implications for ice behavior. J. Glaciol. 47 (158), 397–411.
Wellner, J.S., Heroy, D.C., Anderson, J.B., 2006. The death mask of the Antarctic Ice Sheet: comparison of glacial geomorphic features across the continental shelf. Geomorphology 75, 157–171.
Zagorodnov, V., Nagornov, O., Scambos, T.A., Muto, A., Mosley-Thompson, E., Pettit, E.C., Tyuflin, S., 2012. Borehole temperatures reveal details of 20th century warming at Bruce Plateau, Antarctic Peninsula. Cryosphere 6, 675–686.